Helsinki University of Technology
Department of Electrical and Communications Engineering
Optoelectronics Laboratory
Espoo 2004

ADVANCED FIBER COMPONENTS FOR OPTICAL NETWORKS

Kalle Ylä-Jarkko

Thesis for the degree of Doctor of Science in Technology to be presented with due permission for public examination and debate in Auditorium S4 at Helsinki University of Technology, Espoo, Finland, on the 27 of May, 2004, at 12 o'clock noon.

Helsinki University of Technology
Department of Electrical and Communications Engineering
Optoelectronics Laboratory

Helsinki University of Technology
Optoelectronics Laboratory
P.O. Box 3000
FIN-02015 HUT, Finland

ISBN 951-22-7129-x

Otamedia Oy

Espoo 2004

Abstract

Due to the tremendous growth in data traffic and the rapid development in optical transmission technologies, the limits of the transmission capacity available with the conventional erbium-doped amplifiers (EDFA), optical filters and modulation techniques have nearly been reached. The objective of this thesis is to introduce new fiber-optic components to optical networks to cope with the future growth in traffic and also to bring down the size and cost of the transmission equipment. Improvements in performance and in scalability of the optical networks are studied through simulations and experimental network set-ups.

High-power single-mode laser sources operating at 980 nm are important in pumping EDFAs and Raman amplifiers. In this thesis, two new practical, fiber-coupled configurations of stable high-power cladding-pumped Yb-doped fiber sources operating at 977 nm are presented: a fiber laser and an ASE (amplified spontaneous emission) or superfluorescent source. Sources are based on high numerical aperture Yb-doped jacketed air-clad fiber and high brightness pump diodes.

L-band EDFAs are used to expand amplification bandwidth beyond the C-band wavelengths. Traditional L-band EDFAs are costly devices, which are core-pumped with expensive high-power single-mode diodes. Cladding-pumping technology brings down the cost of the pump diodes in L-band EDFAs, since high-power but low-cost multimode pump diodes can then be used. Additionally, the flexibility in designing erbium-doped fiber is improved. In this thesis, a new design for L-band EDFA based on GTWave cladding-pumping technology is introduced. Simultaneous noise reduction and transient suppression in the amplifier is achieved by using a gain-clamping seed-signal.

To increase the spectral efficiency of the optical transmission systems optical filters having square spectral response and linear phase, leading to zero dispersion both in-band and out-of-band, are required. The application of inverse scattering technique in conjunction with advanced fiber Bragg grating writing technique significantly reduces in-band dispersion and greatly improves grating characteristics. In this thesis, the in-band and out-of-band dispersion penalty of a cascade of linear-phase fiber Bragg grating (FBG) filters is experimentally measured and compared to the results with conventional apodized FBG filters.

Fiber Bragg grating based distributed feedback fiber lasers (DFB FL) are attractive alternatives to semiconductor lasers. Output power and efficiency of DFB FLs can be significantly increased by using a master-oscillator-and-power-amplifier (MOPA) configuration, consequently degrading optical signal to noise ratio (OSNR) and RIN of the master source. These trade-offs are studied in several MOPA configurations using core-pumped and cladding-pumped EDFAs as power amplifiers and compared to the results with a high-power stand-alone DFB-FLs, i.e. DFB FLs pumped with a high-power pump source.

Finally, the performance and scalability of a bidirectional and a high-density metropolitan WDM ring networks is analyzed. Results show that the scalability limitation imposed by the amplified RIN arising from the Rayleigh backscattering in bidirectional WDM ring networks can be avoided by using low gain shared-pump EDFAs and directly modulated transmitters. In high-density metropolitan WDM networks based on non-zero dispersion shifted fibers the main limiting nonlinearity is four-wave mixing. In metropolitan areas distributed Raman amplification (DRA) is the most effective means reduce the effect of four-wave mixing.

Preface

The research work for this thesis has been mainly carried out in the amplifier team of Southampton Photonics, Inc. during the years 2001-2003. Part of the work has also been carried out in Photonics group at the VTT Microelectronics Centre between the years 1999-2001.

I am grateful for several persons who have made it possible to write this thesis. To be able to carry out this kind of work one needs a special kind of working facilities and resources. I would like to express my gratitude to the executive management of Southampton Photonics, Inc. and especially Chairman of the Board professor David Payne and the CEOs Don Spalinger, Barry Dickman, and David Parker for providing the facilities and resources to carry out the research work. I would also like to thank Matti Leppihalme, the leader of the Photonics group at VTT and Jouni Heleskivi, the leader of the VTT Microelectonics Centre for the opportunity to begin the work in the fascinating field of photonics. I am also grateful to Corelase Oy and especially to Harry Asonen for giving me the push and motivation to finalize the writing of the thesis.

I have been enormously lucky to work with innovative supervisors and mentors. Especially, I am grateful for the opportunity to have worked with exceptionally inspiring scientists Prof. Anatoly Grudinin and Prof. Michalis Zervas. They have guided me through most of the research work included in this thesis and have given me a lot of support and encouragement throughout the work. Dr. Johan Nilsson has given a lot of advice in preparation of the manuscripts. Dr. Simo Tammela is recognized for leading me into the world of innovative thinking and scientific reasoning.

There have been also numerous colleagues that have provided help and support in preparing this thesis. Dr. Shaif-ul Alam, Dr. Mike Durkin, Dr. Ian Barry and Dr. Louise Hickey have provided invaluable help in making components needed in the measurements. I would also like to thank the whole amplifier team of Southampton Photonics, who have supported me in various problems related to optical, mechanical and electronic design of the amplifiers and fiber lasers in publications I, II, IV and VI.

Numerous people from Optical Research Centre of Southampton University, Nokia Networks, Nokia Research Center, Teleste Ltd., Metrology Research Institute of Helsinki University of Technology and VTT Microelectronics Centre have generously loaned measurement equipment and shared their knowledge on optical communications.

Finally, I would like to thank my loving wife, Mervi and children, Elias and Enni, for the patience and support they have given me during the sometimes very difficult and demanding writing periods.

List of publications

I R. Selvas, K. H. Ylä-Jarkko, S. A. Alam, P. W. Turner, J. Moore, J. K. Sahu, L. B. Fu, J. N. Jang, J. Nilsson, and A. B. Grudinin, "High power, low noise Yb-doped cladding-pumped three-level fiber sources at 980 nm," *Optics Letters*, Vol. 28, pp. 1093-1095, July 1, 2003

II K. H. Ylä-Jarkko, C. Codemard, J. Singleton, P.W. Turner, I. Godfrey, S.-U. Alam, J. Nilsson, J. Sahu and A. B. Grudinin, "Low noise intelligent cladding-pumped L-band EDFA," *IEEE Photonics Technology Letters*, Vol. 15, pp. 909-911, July 2003.

III K. H. Ylä-Jarkko, M. N. Zervas, M. K. Durkin, I. Barry and A. B. Grudinin, "Power penalties due to in- and out-of-band dispersion in FBG cascades," Journal of Lightwave Technology, Vol. 21, pp. 506-510 , June 2003.

IV K. H. Ylä-Jarkko, and A. B. Grudinin, "Performance limitations of high-power DFB fibre lasers," *IEEE Photonics Technology Letters*, Vol. 15, pp. 191-193, February 2003.

V K. Ylä-Jarkko, S. Tammela, T. Niemi, A. Tervonen and M. Leppihalme, "Scalability of a Metropolitan Bidirectional Multifiber WDM-Ring Network," *Photonic Network Communications*, Vol. 3, pp. 349-362, 2001.

VI K. H. Ylä-Jarkko, S. Alam, and A. B. Grudinin, "Achieving Long Repeaterless Sections in High-Density Metropolitan WDM Networks," *IEEE Photonics Technology Letters*, Vol. 14, pp. 1013-1015, July 2002.

Author's contribution

The results presented in this thesis from publications I-IV and VI are a result of teamwork within the product development teams in Southampton Photonics, Inc. and Optoelectronics Research Centre, University of Southampton. Results from publication V are a result of teamwork within the research group at VTT and co-operation project within industry. The author has prepared publications I-VI.

For publication I, the author carried out all the measurements to characterize the fiber sources. He also developed a measurement set-up to characterize the relative intensity noise of high power fiber lasers.

For publication II, he generated the idea to use a clamping signal to suppress the unwanted transient effects under the channel add/drop operation and simultaneously to improve the performance of the amplifier. He is also responsible of the optical design and building of the amplifier. Measurement set-ups were built by him and he participated in all the measurements.

For publication III, the author designed and built the power penalty measurement set-ups to characterize the fiber Bragg gratings. He conducted all the power penalty measurements and analyzed the bandwidth utilization factor for all the measured gratings.

For publication IV, the author constructed the measurement set-ups and conducted all the measurements.

For publication V the author partly designed and constructed the measurement test-beds. He developed the simulation software to analyze the scalability of the network and built the network nodes and amplifiers in the test-bed.

The design, construction and measurements of the test-bed in publication VI were done by the author. The testing of the Raman fiber laser was partly done by the author. The measurements to characterize the nonlinearities and transmitter characteristics were done by the author.

The results in this thesis have also been presented in several international conferences.

Table of contents

Abbreviations and acronyms

ASE	Amplified spontaneous emission
AWG	Arrayed waveguide grating
B	Boron
BER	Bit-error rate
BU	Bandwidth utilisation
CATV	Community antenna television
C-band	Conventional wavelength band
DC	Double cladding
DFB	Distributed feedback
DFB FL	Distributed feedback fiber laser
DLP	Discrete layer peeling
DRA	Distributed Raman amplification
DRB	Double Rayleigh backscattered
DWDM	Dense wavelength division multiplexing
ECOC	European Conference on Optical Communication
EDF	Erbium doped fiber
EDFA	Erbium doped fiber amplifier
Er	Erbium
FBG	Fiber Bragg grating
FWHM	Full-width half-maximum
FWM	Four-wave mixing
Gb/s	Gigabits per second
Ge	Germanium
GLM	Gelfand-Levitan-Marchenko
JAC	Jacketed air-clad fiber
L-band	Long wavelength band
MAN	Metro area network
MOPA	Master-oscillator-power amplifier
NA	Numerical aperture
Nd	Neodymium
NF	Noise figure
NRZ	No return to zero
NZ-DSF	Non-zero dispersion shifted
OFC	Optical Fiber Communication Conference
PRBS	pseudo-random bit stream
RIN	Relative intensity noise
RO	relaxation oscillation
RZ	Return to zero
Rx	Receiver
SBS	Stimulated Brillouin scattering
SDM	Spatial division multiplexing
SM	Single-mode
SPM	Self-phase modulation
SNR	Signal to noise ratio

Tb/s	Terabits per second
TDM	Time division multiplexing
Tx	Transceiver
WDM	Wavelength division multiplexing
XPM	Cross-phase modulation
Yb	Ytterbium

1 Introduction

To meet the rapidly growing data traffic demands, the capacity of optical transmission systems has expanded tremendously within the last decade. Currently service providers are considering of deploying dense-wavelength division multiplexing (DWDM) systems exceeding terabit capacity. In laboratories several experiments with multiterabit transmission systems with channel capacity of 40 Gb/s have been carried out [1]-[4]. The record-breaking systems in a single fiber have achieved over 10 Tb/s [1],[2] with a transmission distance up to 10000 km demonstrating the huge development in expanding the bandwidth of optical amplifiers and improving the spectral efficiency of the optical transmission systems [3],[4]. With these experiments the capacity available with the bandwidth of erbium-doped fiber amplifiers (EDFA), optical filters and conventional modulation techniques has been achieved and new technologies are needed not only to cope with the future growth in traffic but also to bring down the size and cost of the long haul transmission equipment.

As the long-haul transmission systems are being upgraded to be capable of transmitting several terabits/s, a bottleneck in the delivery of data services to access networks has been created. To relive the bottleneck, transmission speed and transmission distances in the metropolitan area networks have been increasing. Additionally, in metropolitan area networks the ratio on network nodes per transmission distance and patching collocations is higher than in long-haul network. [V,VI] These elements coupled with the cost pressure for edge services, force system integrators to change design rules and consider advanced, high specification components and amplification schemes at lower price to reduce the capital and operation expenditure of the transmission equipment and at the same time to increase the optical bandwidth and the spectral efficiency of the metropolitan optical networks.

The need for capacity in long haul and metropolitan area systems drives not only the amplification requirements, i.e. output power, gain flatness, gain bandwidth, but also the required number of EDFAs in the network. Conventionally, EDFAs have been stand-alone devices, which in low channel count systems are individually pumped by traditional laser diodes and packaged separately. In trunk systems having hundreds of channels, they are pumped by up to six pump diodes increasing the cost and complexity of the device. The most obvious way to reduce the cost of amplifiers is to share pump sources between several EDFAs (shared-pump EDFAs) or to reduce the number of pumps in a single amplifier. This can be done in several ways, most straightforwardly by developing high power single-mode pump sources [8]-[12]. Such sources are also very desirable as initial pumps for Raman amplifier.

In addition to developing new pump sources and pumping schemes for optical amplifiers, the cost of optical amplification can also be brought down by broadening the amplification bandwidth and developing amplifiers that on their own offer a range of attractive features improving the performance of the transmission systems. L-band transmission window (1570-1605 nm) has been of special interest for optical transmission system designers not only because it offers a direct route to expand the transmission capacity of the current optical systems operating in C-band (1525-1565 nm) but also because it gives more flexibility in system design. L-band EDFAs operate at low average inversion and thus have intrinsically flat gain and low gain ripple compared to the C-band (1530-1565 nm) EDFAs. L-band transmission window has also higher four-wave mixing threshold in widely deployed dispersion shifted fibers and non-zero dispersion shifted fibers, and flatter third order dispersion and

consequently more flexible dispersion compensation. Despite these obvious benefits wide deployment of L-band EDFAs has so far been hindered by the fact that they are costly and power-hungry devices, which require multiple high-power single-mode pump diodes at 980 nm and 1480 nm. Thus, new improved designs lowering considerably the cost of pumping are required.

Besides broadening the gain bandwidth of the optical amplifiers the transmission capacity of the WDM networks can be increased by improving the spectral efficiency of the system. Spectrally efficient, high-density long-haul networks require optical filters, which have nearly ideal performance. These filters have square spectral response and linear phase, leading to zero dispersion, both in-band and out-of-band. In order to have scalable metro network architectures optical filters having low dispersion and low insertion loss both for the add/drop and express channels, good crosstalk characteristics, and wide usable bandwidth are needed.

In high-density WDM networks laser sources with extremely high wavelength accuracy and stability are important to achieve stable performance of the system over long periods. Currently, the wavelength of a diode laser is controlled by stabilizing the temperature. However, with ultradense channel spacing and in trunk systems the accuracy of the active temperature control is not sufficient enough and external methods based on f.ex. multiwavelength meters and Fabry-Perot interferometers are required. Since making small and cost-effective 40 Gb/s transmission equipment is a crucial issue today, there is room for alternative transmitter solutions. These transmitters should have high wavelength accuracy and stability, low relative intensity noise (RIN), high output power and high wall-plug efficiency. Coupled with the high specification performance they should also impose characteristics such as low production costs, good integrability with fiber optics based transmission systems and fabrication simplicity.

1.1 Aims of the thesis

This thesis is divided into two themes. Firstly, new fiber-optic components for optical networks are introduced and improvements to the performance of advanced fiber components are suggested and experimentally studied. Secondly, the performance and scalability of different metropolitan WDM network architectures is studied and new methods to increase the network scalability by the use of proper network engineering and the choice of optimized fiber optic components are presented.

High-power laser sources operating on a single transverse mode at 980 nm are important for pumping erbium-doped fiber amplifiers. To develop pump sources having higher output power at lower cost, cladding pumped Yb-doped fiber lasers operating at ~977 nm have been the subject of significant technical and experimental activity in recent years. Despite obvious attractions of such sources there have been no reports on practical, user-friendly, devices. In this thesis two new practical, fiber coupled configurations of stable high-power cladding-pumped Yb-doped fiber sources operating at 977 nm are presented: a fiber laser and an ASE (amplified spontaneous emission) or superfluorescent source.

Compared to the core-pumped devices cladding-pumping offers greater flexibility in erbium-doped fiber design and brings down the cost of the pump diodes, since high-power, but low-cost multimode pump diodes can then be used. In this thesis, a new design for L-band EDFA based on GTWave cladding-pumping technology is introduced. The suppression of unwanted transient effects under the channel add/drop

operation and the performance of the amplifier are enhanced by using a gain-clamping technique.

Cascading of optical filters imposes significant limitations on scalability of optical networks because of channel crosstalk and in-band dispersion resulting in signal distortion. The application of inverse scattering technique in the FBG design in conjunction with advanced fiber Bragg grating writing technique significantly reduces in-band dispersion and greatly improves grating characteristics. In this thesis, the in-band dispersion penalty of a cascade of linear-phase fiber Bragg grating (FBG) filters is experimentally measured and compared to the results with conventional apodized FBG filters. Additionally, dispersion penalty measurement to quantify the penalty on a dropped channel caused by a cascade of five adjacent channel gratings is introduced.

In high-density networks and CATV systems laser sources having high wavelength accuracy and stability, low relative intensity noise (RIN), high output power and high wall-plug efficiency are required. Fiber Bragg grating based distributed feedback fiber lasers (DFB FL) have all attributes to make them almost an ideal source for both WDM and CATV systems. However, high output powers (>40 mW required for CATV) directly from DFB FLs have not been easy to achieve due to short device length and low single-pass gain, which results in relatively low slope efficiency of the single frequency fiber lasers. Output power and efficiency can be significantly increased by using a master-oscillator-and-power-amplifier (MOPA) configuration, consequently degrading optical signal to noise ratio (OSNR) and RIN of the master source. These trade-offs are studied in several MOPA configurations using core-pumped and cladding-pumped EDFAs as power amplifiers and compared to the results with a high-power stand-alone DFB-FLs, i.e. DFB FLs pumped with a high-power pump source.

The scalability of WDM networks depends on effects such as fiber attenuation, node losses, noise accumulation, fiber and component chromatic dispersion, filter concatenation, crosstalk and fiber non-linearities. Therefore, the design of transparent WDM networks requires careful engineering and the use of optimised optical layer components and fiber. In this thesis, the scalability of a metropolitan multifiber WDM-ring network with shared-pump EDFAs using bi-directional transmission is analyzed. The analysis is carried out by using a bi-directional transmission model for optical networks and by building an experimental network. The limitations imposed by stimulated Brillouin scattering (SBS) and four-wave mixing (FWM) in high-density metropolitan WDM networks under worst-case non-linear interaction conditions are also studied and their implications on the length of repeaterless sections are quantified. Furthermore the practicality of distributed Raman amplification in the metropolitan optical networks based on non-zero dispersion-shifted transmission fiber (NZ-DSF) is experimentally demonstrated.

2 Yb-doped fiber based pump sources for optical amplifiers and fiber lasers

2.1.1 Ytterbium-doped silica fiber lasers

Since the introduction of the first Yb^{3+}-doped silicate glass, Yb^{3+} was overshadowed several decades by Nd^{3+} as a laser active ion. However, along with the introduction of cladding-pumped fiber lasers Yb^{3+} has become the preferred choice as doping material for high power fiber lasers. This is mainly due to very efficient operation of Yb-doped fiber lasers and very broad absorption and emission spectrum of ytterbium-doped silica fibers offering a broad range of pumping and lasing wavelengths. The efficient operation of Yb-doped fiber lasers arises from the non-existent excited state absorption at pump and laser wavelengths. Ytterbium has also a large energy gap between the ground level manifold and excited manifold, which prevents the nonradiative decay of excited state via multiphoton emission and concentration quenching [5]. The output powers from Yb-doped fiber lasers have recently increased tremendously. In the recent experiments hundreds of watts have been achieved from single-mode devices making fiber lasers serious contenders for lamp- and diode-pumped Nd:Glass lasers in material processing [6],[7]. However, in the wavelength range of 970-980 nm, which is especially attractive for pumping EDFAs, and other devices based on rare-earth-doped fibers there has been much less success in the development of efficient devices operating even at the 1 W level of fiber coupled output power [8]-[10].

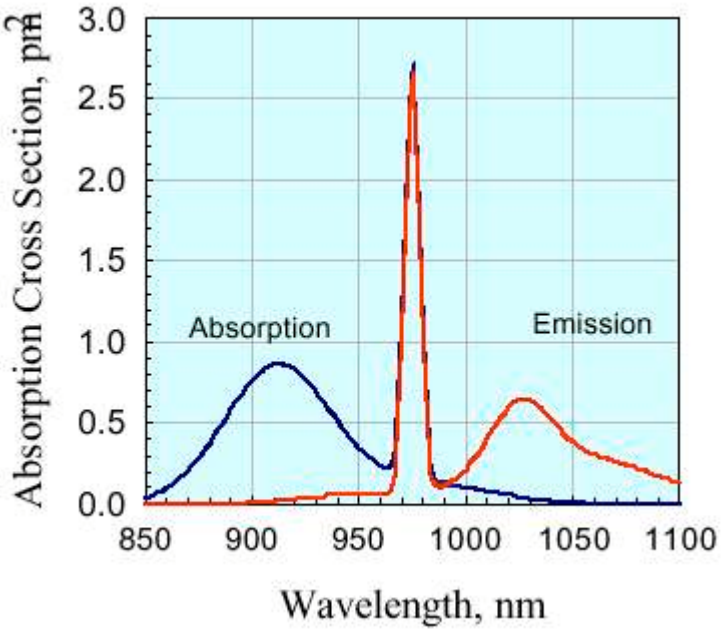

Figure 1. Absorption and emission cross-sections of Yb^{3+}-ion in germanosilicate glass. [13]

Ytterbium-ions in silica host have two emission peaks centered around 980 nm (three-level transition) and 1040 nm (quasi-four level transition) as shown in Fig. 1. The difficulty to achieve an efficient laser operating at the three level regime arises from the large absorption peak also located around 977 nm. Hence, over 50% Yb-ion excitation is required to bleach the re-absorption loss of the laser transition whereas only 5% excitation is needed in the quasi-four level regime. With traditional double-

clad fiber structures and low-brightness pump sources such high inversion cannot be achieved, at least not in an efficient device, as the overlap between the pump field and doped core is too small [14]. This can be illustrated by considering the required critical pump power to bleach the gain medium at a particular point in the fiber given by

$$P_{cr} = \frac{A_{core} h \nu_p}{\eta_{pump}\left(\frac{\sigma_{es}\sigma_{ap}}{\sigma_{as}} - \sigma_{ep}\right)\tau}. \quad (1)$$

A_{core}, h, ν_p and τ denote the core area, Planck's constant, pump laser frequency and the upper level lifetime. Respectively σ_{es} and σ_{as} are the emission and absorption cross-sections at the signal wavelength and σ_{ep} and σ_{ap} are the emission and absorption cross-sections. Some of the pump light in the fiber travels in the region outside of the signal core, this is taken into account with the pump overlap factor η_{pump}. Figure 2 shows the dependence of the critical power (threshold power) on the inner-cladding from Eq. (1). For a practical single-mode device having a threshold below 500 mW, the inner-cladding diameter should be between 20-33 μm. Traditional low-brightness pump diodes delivering output power of 1.5 – 2.5W are typically coupled to either 65 μm or 100 μm fiber. With such pump sources the lasing threshold for the fiber laser can barely be reached and hence they are not suitable for cost-effective realization of fiber based 980 nm pump sources as shown by the dashed arrows in Fig. 2.

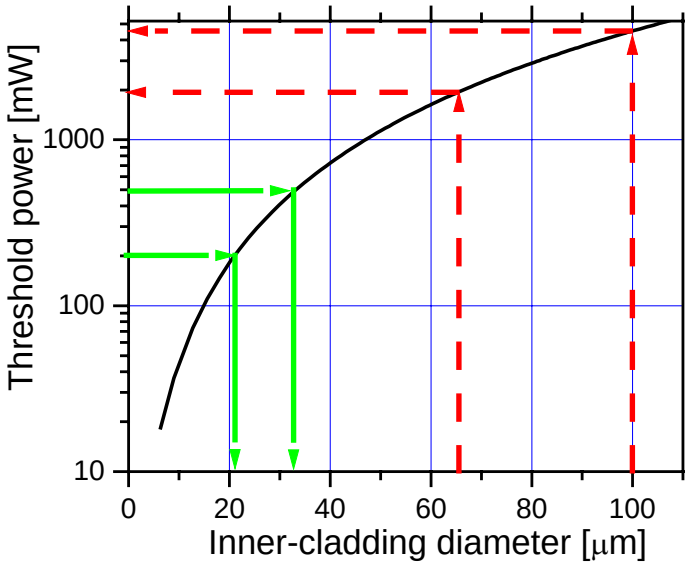

Figure 2. Dependence of the threshold power on the inner-cladding diameter. Solid arrows indicate the inner-cladding diameter for a practical single-mode 980 nm fiber laser. Dashed line shows the threshold for a fiber laser with traditional, low-brightness pumps.

In addition to low threshold power an efficient laser requires also high slope efficiency with respect to the launched pump power. In cladding-pumped fiber lasers low overlap between the gain medium and pump field yields typically long device lengths until the lasing threshold is reached. To shorten the device length fibers have large dopant concentration. These characteristics give rise to special problems for fiber sources operating at 980 nm. Before reaching the lasing threshold at 980 nm,

915 nm pumping induces high net gain at longer wavelengths increasing the amount of amplified spontaneous emission (ASE) noise. This degrades the optical signal-to-noise ratio and reduces the slope efficiency of the laser but most detrimentally creates oscillations between the 980 nm and 1030-1040 nm lasing wavelengths.

The competition between the gain build-up at 980 nm and at longer wavelengths can be considered in detail by finding an expression for gain in Yb^{3+}-doped fibers. In homogenously broadened gain medium, the gain in decibels can be expressed by [14]

$$G(\lambda) = 4.343 N_0 A_d \Psi_d(\lambda)\{[\sigma_{es}(\lambda) + \sigma_{as}(\lambda)]n_2 - \sigma_{as}(\lambda)\}L\,. \qquad (2)$$

Here N_0 is the concentration of the active ions, L is the fiber length, and σ_{es} and σ_{as} are the emission and absorption cross-sections, and n_2 is the fraction of active ions that are excited. The normalized modal intensity averaged over the dopant area A_d is denoted by Ψ_d. From Eq. (2) the expression for the undesired gain at 1030 nm can be deduced [14]

$$G^{1030} = 0.25 G^{975} + 0.72 \beta \alpha_p\,, \qquad (3)$$

where α_p is the pump absorption and $\beta = \dfrac{\Psi_d^s}{\Psi_d^p} = \dfrac{A_{cladding}}{A_{core}}$. Hence, the gain at 1030 nm grows rapidly as the pump absorption is increased. The amount of 1030 nm gain can be reduced by having a low inner-cladding to core ratio and by removing dopants from the core and therefore reducing the amount of Ψ_d^s without effecting Ψ_d^p. This can be realized by introducing a ring with Yb^{3+}-ions around the single-moded core (ring-doping) [14].

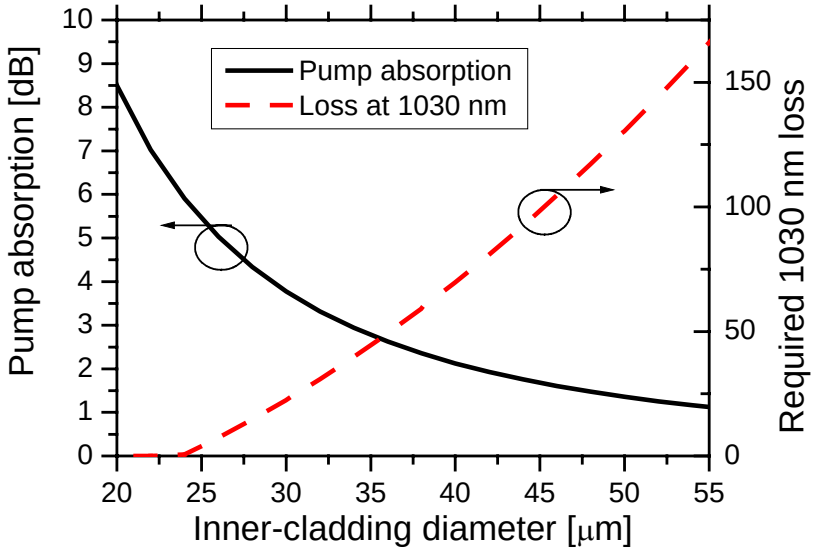

Figure 3. Pump absorption limit (solid line) as a function of inner-cladding diameter. The amount of pump absorption is set by the maximum 1030 nm gain (40 dB). The additional loss required to suppress the ASE build-up at 1030 nm as a function of inner-cladding diameter. Maximum suppression from wavelength-selective end reflectors is about 50 dB.

To have a practical pump source, the gain at 1030 nm needs to be below 40 dB in order to avoid the lasing effects caused by Rayleigh backscattering and reflections from splices. The build-up of ASE at 40 dB of gain sets also the limit on the amount of pump absorption in the fiber. Pump absorption limit can be calculated from Eqs. (1) and (3). For the calculations the gain at 1030 nm, G^{1030} is set at 40 dB and the

single pass gain to achieve lasing, G^{980}, is 7 dB (assuming a laser cavity with 99% reflecting mirror in the other end and Fresnel reflection from the flat cleaved fiber in the other end). The pump absorption limit for such a single-mode 980-nm fiber laser is shown in Fig. 3. From the figure it can be deduced that for a laser having a threshold of 200-500 mW, i.e. inner-cladding diameter 20-33 μm, the required pump absorption is approximately 3…6 dB. Additionally, in order to suppress the pump through to acceptable limits and to avoid the quenching effects in heavily doped Yb-doped fibers a practical value for pump absorption is 6 dB (75%) [14]. From the Fig. 3, it can be seen that that the pump cladding diameter for the laser is 24 μm. Inner-cladding diameter of the doped fiber can be increased up to 35 μm by placing wavelength selective end reflectors into the cavity as shown in Fig. 3.

2.1.2 Jacketed air-clad Yb-doped fiber

The threshold and the unwanted long wavelength gain of the cladding pumped Yb-doped fiber sources can be most cost-effectively reduced by designing a fiber with a small inner-cladding to core ratio and high NA to maximize the pump launch efficiency. By introducing silica-air outer cladding in double-clad fibers the NA of the inner-cladding can be increased enabling the decrease of the inner-cladding diameter without sacrificing the efficiency of the pump coupling. This increases the overlap between the pump and signal fields and hence the output power from the diode-pumped fiber lasers can be raised without boosting the pump power [15].

Several types of air-clad fibers have been demonstrated in the literature [14]-[18]. Most straightforward method is to remove the second cladding from the fibers and use bare fibers coiled together [16]. The outer diameter of the fiber is equal to the diameter of the inner-cladding. However, fibers with outer diameter in the region of 20-33 μm are very difficult to handle and are prone to contamination. These problems can be avoided by introducing cladding-pumped fibers with silica-air secondary cladding based on the fabrication methods that are also used for making silica-air optical fibers (photonic crystal or holey fibers) [19],[20].

First cladding pumped silica-air fiber was described in Ref [15]. This “candy cane” type of fiber was manufactured by confining the high-index inner-cladding and doped core within a supporting tube by means of a connection element. Within the structure the secondary cladding consists of air apart from the fluorine-doped silica rod in between the inner-cladding and the supporting tube. Numerical aperture of 0.3 was achieved from this structure for fiber lengths up to 50 cm but only 0.2 for longer fiber lengths. Additionally, the fiber type suffers from the leakage of photons through the connecting silica rod making the structure very inefficient for the use of high-power fiber lasers.

In order to realize an inner-cladding having a higher NA than that of the conventional double-clad fiber (NA=0.35…0.47) based on polymer secondary-cladding, a jacketed air-clad (JAC) geometry first described in [17] can be used. This approach is similar to the “candy cane” structure and it is based on robust reproducible conventional silica fiber technology. High NA of the inner-cladding is achieved by having a mesh of different size of silica capillary tubes stacked around a rod with an Yb-doped core inside a silica jacket [18]. With this technology an inner-cladding NA higher than 0.7 can be achieved. Figure 4 shows a cross-section of the Yb-doped JAC fiber, with white light launched into the inner cladding and emerging through the imaged end. The multimode inner cladding is supported by a thin glass mesh with a wall thickness

comparable to the wavelength. This results in very low pump leakage and hence high numerical aperture of the inner cladding.

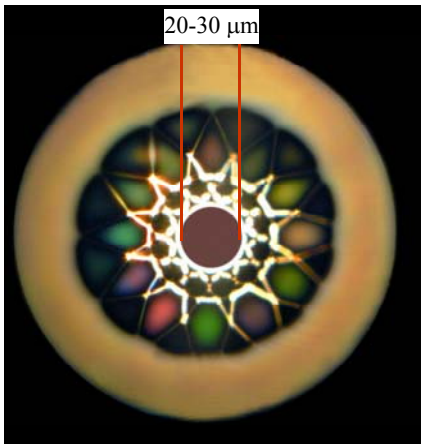

Figure 4. Cross-section of jacketed air-clad (JAC) fiber. Inner cladding diameter 20 µm, NA 0.7. Core diameter is 9 µm, NA=0.1.

2.1.3 Jacketed-Air clad cladding pumped fiber sources at ~980 nm

Yb-ions have a relatively narrow emission bandwidth (~4 nm) centered around 977 nm. Hence, a spectrally concentrated, high power output can be achieved from a simple ASE source, as well as from a laser using broadband feedback from a mirror or wavelength-selective narrowband reflectors such as fiber Bragg gratings. The configuration of the fiber sources that were used are shown in Fig. 5. For the ASE source, the Yb-doped JAC-fiber (length 1.2 m) was spliced to a single-mode fiber (core diameter 6 µm, NA=0.14) with an angled output facet that suppressed the feedback. This makes the output nearly uni-directional even with a simple perpendicular cleave (4% reflecting) in the pump launch end of the fiber. For the laser configuration, a fiber Bragg grating with reflectivity ~10% (FWHM = ~0.2 nm) was spliced to the output end of the JAC-fiber, while the laser was pumped through a broadband dichroic mirror that provided feedback in the other end of the cavity. Both sources used a 915 nm laser diode pump module. Each pump module contained two 100 µm broadstripe laser diodes with 4 W of output power. The diodes were coupled to a 30-µm, 0.3 NA fiber. The total fiber-coupled output power from pump module was 5 W. [I]

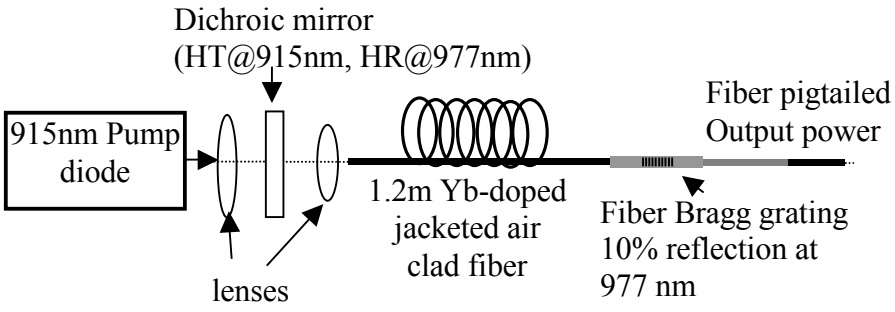

Figure 5. Schematic configuration of the JAC fiber laser. For the ASE source, the Yb-doped JAC-fiber was spliced to another fiber with an angled output facet that suppressed feedback. [I]

The output power characteristics of the sources are shown in Fig. 6. The fiber laser has higher output power (1.4 W) and slope efficiency (68%) than the ASE-source. Another additional benefit of the laser configuration is that the output is less sensitive

to back-reflection. The drawback of the laser configuration compared to the ASE-source is a more complex structure. The output power of the ASE-source is 1.2 W and the slope efficiency is 37%. The benefit of ASE-source is a simple structure, as no external feedback is required to produce emission at 977 nm. Drawbacks of the ASE-source are lower efficiency and inherent sensitivity to back-reflections (isolators for 980 nm do exist, but they are bulky, lossy, and expensive). [I]

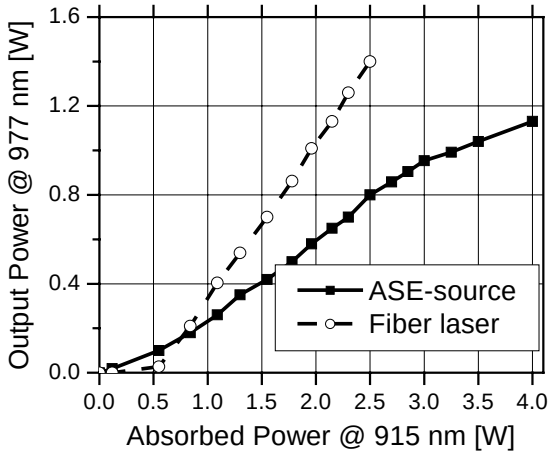

Figure 6. Output power and slope efficiency of the JAC fiber laser and ASE-source as a function of absorbed pump power. Threshold and slope efficiency for the ASE source are 120 mW and 37%. For the fiber laser they are 400 mW and 68%. [I]

The output spectra of the sources are shown in Fig. 7. Suppression of emission at ~1040 nm is more than 20 dB for both sources. The spectral width of the ASE source is 3 nm and the center wavelength is situated at 977 nm, which is practically at the peak of the ~980 nm absorption band of erbium-ions in silica glass. The spectral width of the fiber laser was 0.5 nm, mainly determined by the characteristics of the reflective grating. [I]

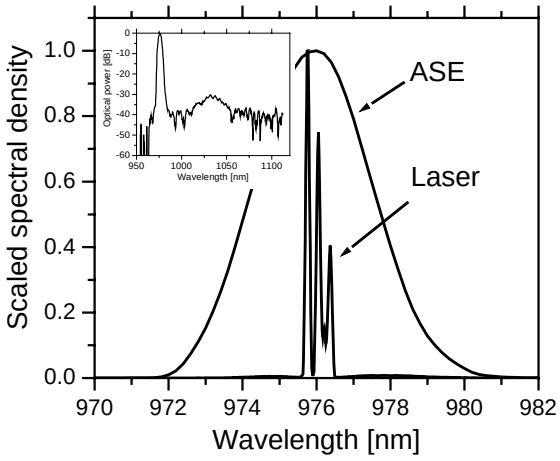

Figure 7. Output spectra for the fiber laser and the ASE source. [I]

In some applications, such as pumping of DFB fiber lasers (DFB FLs), the temporal stability of Yb-doped fiber-based pump source is as important as the wall-plug efficiency and output power. Figure 8 shows the RIN spectrum of the 977 nm fiber laser and ASE sources. The ASE-source has no cavity and hence its RIN is white, without any peaks arising, e.g., from relaxation oscillations or other cavity effects.

The RIN of the ASE-source is below –130 dB/Hz and thus does not generate any extra contribution to RIN of the DFB FL. [I]

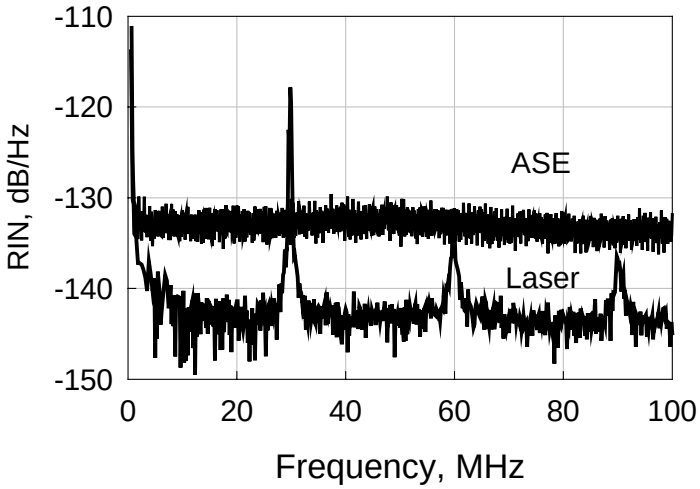

Figure 8. Relative intensity noise graphs for the fiber laser and ASE fiber source operating at~ 977 nm. [I]

Fiber laser pump source has several RIN peaks. The relaxation oscillation peak occurs at 450 kHz at a RIN level of –110 dB/Hz. The RIN peak at 30 MHz is dependent on the cavity length and hence on the position of the grating output coupler. In the measurements the cavity length was 3.3 m. The additional peaks in the RIN spectrum are harmonics of the beat frequency of the longitudinal modes within the laser cavity. Outside the peaks the RIN of the fiber laser is very low and limited only by the sensitivity of the measurement device (~ –145 dB/Hz). [I]

3 GTWave cladding pumping technology for L-band amplifiers

L-band amplifiers exploit the long tail of the erbium gain band far away from the emission peak (~1530 nm) and hence have 3-4 times lower emission and absorption cross-sections compared to the C-band EDFAs. Figure 9 shows the energy levels of erbium ion and also illustrates the generation of L-band gain in erbium-doped fibers. Large amount of amplified spontaneous emission (ASE) noise in 1530-1560 nm band is generated in the input portion of the fiber. As the length of the Er-doped fiber is increased this ASE-noise is reabsorbed creating gain at longer wavelengths. Long device length is the origin of the poor power conversion efficiency of L-band amplifiers, because both the pump and signal fields experience high propagation and scattering losses and also large amounts of wasteful backward propagating ASE-noise is generated.

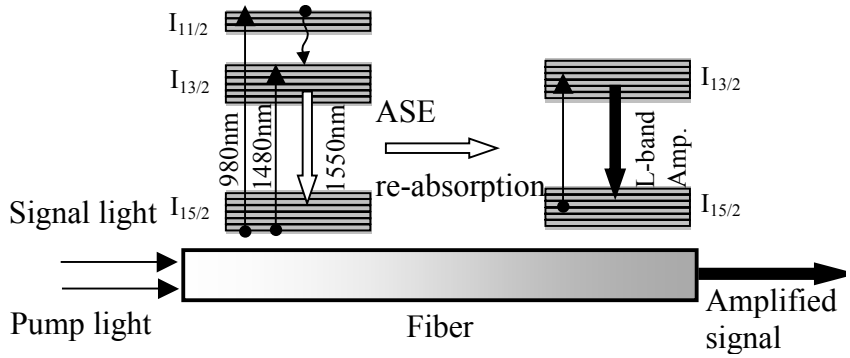

Figure 9. Energy level diagram of Er^{3+}-ion and schematic operation principle of L-band EDFA.

Conventionally, L-band EDFAs have been core-pumped devices requiring multiple high-power pump diodes at 980 nm and 1480 nm [22]. There have been several suggestions to improve the efficiency mainly based on either recycling the backward propagating ASE [23],[24] or suppressing the generation of the ASE by using multiple stage configurations, C-band seeds and C-band pumps [25]-[27] and single-mode pumps with wavelength detuned away from the ~980 absorption peak [28]. Unfortunately, these improvements come at a significant cost and the fundamental problem with the small emission cross-sections leads to the use of multiple pump diodes. From this standpoint cladding-pumped L-band EDFAs offer a cost effective alternative to traditional core-pumped devices as low cost, high power multimode pumps can be used. Additionally, cladding pumping offers more flexibility in erbium-doped fiber design [29]. For instance with a proper design of the pump-cladding and core sizes the generation of the backward traveling ASE can be reduced. In cladding-pumped amplifiers the large cladding area results in a more uniform pump power distribution along fiber length preventing build-up of short wavelength gain and ASE power [30]. Also with increased doping levels and uniform doping across the doped core, the device length can be made comparable or even shorter than in the core-pumped devices [31].

3.1 Amplifier design and results

Double-clad active fibers consist of a doped single-mode core, a silica inner-cladding with a diameter of several hundred micrometers and a second low index outer-cladding consisting of silicone resin or low index polymer. The NA between the

inner- and outer-cladding is in the range of 0.35–0.47 depending on the refractive index of the coating material. The inner-cladding is used to couple pump radiation from low-brightness multimode pump sources such as high-power diode lasers and diode laser bars and arrays. Typically the overlap between the pump field and doped core is small resulting in long device lengths to absorb the pump radiation. Pump absorption can be enhanced by designing fiber structures where the single-mode core is offset from the center of the circular cladding and where the circular symmetry of the inner-cladding is broken [32].

In this thesis, a new low-cost design for L-band EDFA based on GTWave cladding-pumping technology is used. The fiber amplifier is based on GTWave technology where two or more optical fibers form a fiber bundle, which shares a common external low index coating as shown in Fig. 10(a). All the fibers in the assembly are in optical contact with each other forming a common inner-cladding. The pump light from multimode pump diode(s) is launched into the undoped pump fiber(s) and propagates freely between the fibers in the assembly providing the pump power for the doped core. The pump absorption in the structure is high because the core of the signal fiber is shifted from the center of the common inner-cladding formed by the fibers in the bundle and because of its non-circular symmetry. Further benefit of the structure is that the fibers in the GTWave assembly can be processed independently by stripping of the external coating.

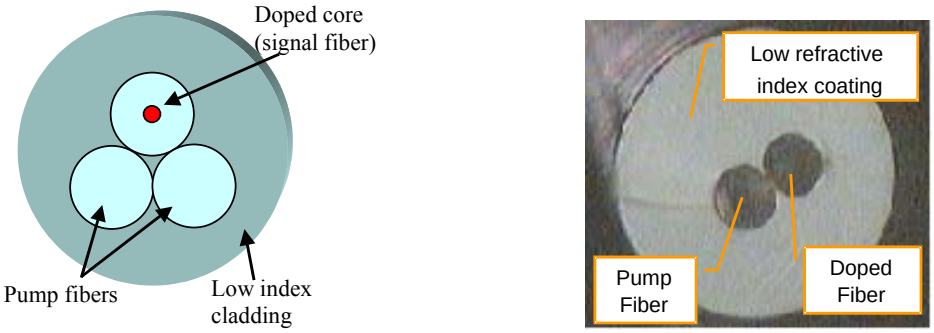

(a) (b)

Figure 10. (a) Schematic cross-section of a GTWave cladding pumped fiber. (b) Cross-section of Er-doped GTWave fiber designed for L-band amplifier.

Figure 10(b) shows the cross-section of the Er-doped GTWave fiber designed for L-band amplifier. In this case the GTWave fiber assembly has two fibers: one core-less, undoped silica fiber used as a pump fiber (outer diameter 60 μm) and one Er-doped fiber with a cut-off wavelength of 1500 nm, absorption of 14 dB/m at 980 nm for light propagating in the core, and core diameter of 10 μm (outer diameter 60 μm). The outer diameters of the fibers and the core diameter of the doped fiber were chosen to maximize the pump confinement within the doped core. The experimental set-up of the amplifier is shown in Fig. 11. The GTWave fiber is 50 m long and is pumped by a 977 nm pump module pigtailed to a fiber with a 50 μm core giving an output power of 1.5 W. For gain clamping, a variable-power control beam at 1564 nm is injected into the core together with the signal. The pump, signal, and gain clamping beams are all propagating in the same direction through the amplifier. This configuration minimizes the noise figure. With 700 mW of absorbed pump power the cladding-pumped GTWave L-band EDFA is capable of delivering 21 dBm of saturated output power. The amplifier exhibits >30 dB gain over 1570-1607 gain band and gain flatness of ± 1 dB as is shown in Fig. 11(b).

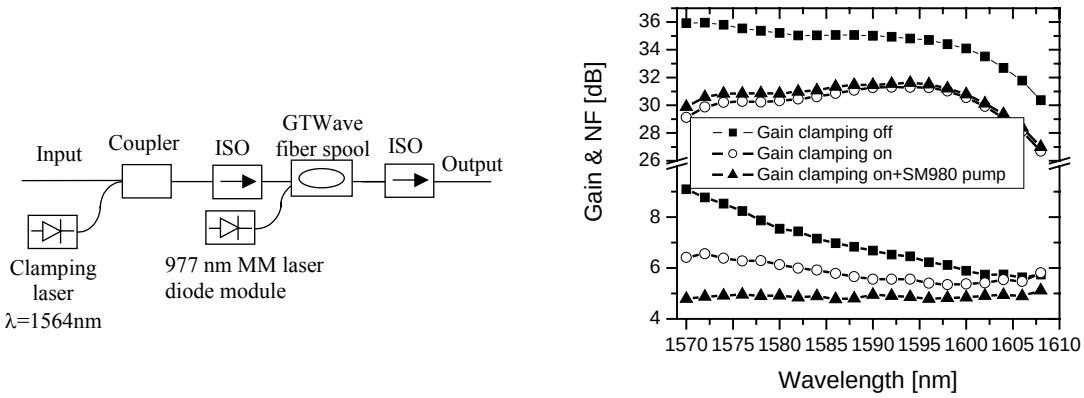

(a) (b)

Figure 11. (a) Schematic layout of the gain-clamped L-band EDFA based on GTWave technology. (b) Gain and noise figure of the cladding-pumped EDFA, as the gain-clamping laser is turned on/off. Input signal power is –20 dBm and the clamping power is –3 dBm [II].

In addition to flat gain and low noise figure an L-band EDFA in WDM systems should be able to offer insensitivity to sudden changes of input power during channel add/drop operation [33]. In L-band amplifiers gain clamping is especially attractive in suppressing the unwanted transient effect because it also reduces the noise figure as is shown in Fig. 11(b). The noise figure is improved by more than 1 dB due to the reduction of the short wavelength gain and the build-up of the backward propagating ASE power. Further improvement can be made by increasing the inversion in the input portion of the fiber, for example, by pumping the EDFA with a single-mode 980 nm pump diode with an optical power of 50–100 mW.

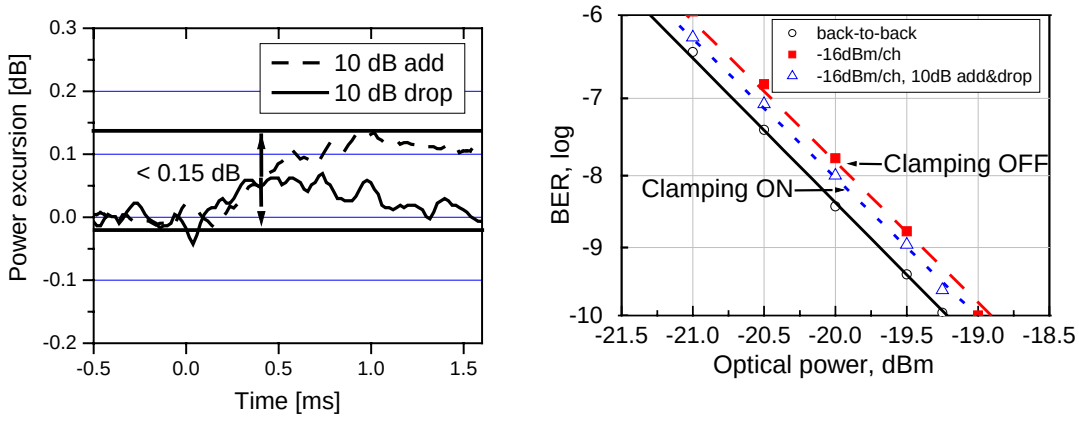

(a) (b)

Figure 12. (a) Transient power excursions of the surviving channel as the optical channels are added and dropped (drop/add ratio 10 dB). (b) BER curves for surviving channel as the input power to the EDFA is constant (no clamping laser) and as the input power is varied by 10 dB (clamping laser on). The total input power to the amplifier is –6 dBm and the power of the surviving channel is –16 dBm. [II]

The transient behavior of the surviving channel in the GTWave L-band EDFA was measured using two sources at 1590 nm and 1595 nm. The input power of the surviving channel (1595 nm) 10 dB drop is –16 dBm. During channel add/drop the power from the clamping laser changes to compensate the increase or decrease in input power, i.e., the clamping laser is turned up as channels are dropped and turned down as channels are added. The dropping/adding of the channels was simulated by a 1590-nm signal modulated at 10 Hz. The transient power excursions of the surviving

channel are monitored by a fast oscilloscope and are shown in Fig. 12(a). The worst-case power excursion for 10 dB add is 0.15 dB, thus verifying the sufficient speed of the transient suppression circuit. Power penalty free operation of the amplifier for 10 dB variations of input power was verified in BER measurements as shown in Fig. 12(b). The reduction of the penalty is attributed to the decrease of noise figure resulting from the C-band injection to the EDFA. [II]

4 Linear-phase fiber Bragg gratings in optical networks

Optical filters having square spectral response and low insertion loss both for the add/drop and express channels are critical components in order to have scalable and spectrally efficient WDM network architectures. In a typical multiwavelength optical network optical signal passes through many network elements, and hence travels through several optical filters before reaching its destination as is illustrated in Figs. 13(a) and 13(b). In metropolitan WDM networks the number of nodes in the network can be as high as 20 and the optical signal begins to degrade due to a variety of signal impairments induced by the amplitude and phase response of the WDM filters. Signal distortions caused by the imperfect amplitude response include effects such as channel crosstalk and signal distortions due to bandwidth narrowing of the pass-band [34]. To minimize these impairments filters should be optimized to have: 1) low insertion loss across the whole pass-band, 2) low crosstalk, i.e. good rejection of the out-of-band signals, 3) sharp and steep edges 4) good spectral structure in the pass-band (e.g. low ripple and good flatness) and outside the pass-band (e.g. reduced side lobes) and 5) wide pass-band.

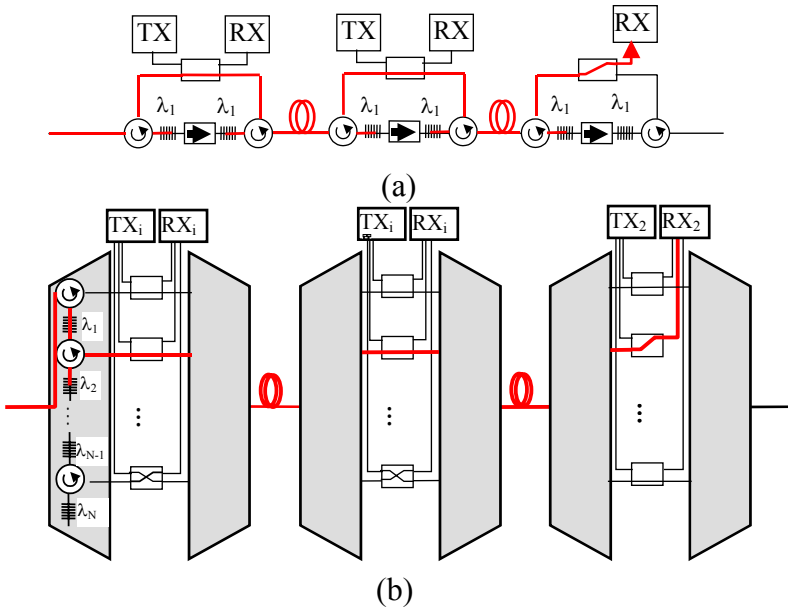

Figure 13. Cascading of FBG filters in WDM add/drop networks. (a) Cascade of M switchable single-channel optical add-drop multiplexers; a channel λ1 can be added at any node and dropped at any subsequent node by setting all the in-between 2x2 switches to the bar state. (b) WDM reconfigurable network with nodes comprising all-grating multiplexer/demultiplexer pairs connected via optical 2x2 switches. This is a multiwavelength extension of the system shown in (a). [III]

Variety of optical filters such as Mach-Zehnder and arrayed waveguide gratings (AWG), dielectric thin-film filters, and fiber Bragg gratings have been used in WDM networks. AWGs suffer from high insertion loss and poorer crosstalk characteristics, although they are as finite impulse response filters ideally dispersion free. Fiber Bragg gratings and thin-film filters are attractive due to their desirable amplitude response, i.e. flat pass-band and low insertion loss. Additional advantage of fiber Bragg gratings is that the reflectivity of the grating can be very strong for a narrow wavelength band with flat-top, low loss reflection spectrum for the drop channels and very sharp

transition at the edges of the pass-band. Hence, the crosstalk, i.e. the amount of residual power from the adjacent channel, is minimized and the loss for the transmitted channels is low. The difficulty in using FBGs (as well as thin-film filters) in large WDM networks has been signal distortions due to dispersive effects in transmission through cascades of filters as the signal is detuned from the filter central, zero-dispersion wavelength. The origin of the dispersion penalty is the direct relation between phase and the change of the amplitude response [35]. As the amplitude response in these filters, often called non-minimum phase filters, changes radically near the pass-band edges, also the phase will change correspondingly leading to a considerable dispersion that ultimately will limit the system performance [36]-[40]. Therefore a significant amount of technical and experimental activity in recent years has been targeted in developing manufacturing and design methods of FBG with a square spectral response and linear phase response [41]-[55].

4.1 Fiber Bragg gratings

Fiber Bragg gratings are manufactured by exposing the core of the optical fiber to a periodic ultraviolet pattern [47]. The resulting index perturbation in the core is a periodic structure that acts as pass-band filter reflecting the light at Bragg wavelength λ_B given by

$$\lambda_B = 2n_{eff}\Lambda, \tag{4}$$

where Λ is the grating period and n_{eff} is the effective refractive index. The index perturbation is described by

$$\delta n_{eff} = n_0 + \Delta n(z)\cos\left\{\frac{2\pi}{\Lambda}z + \theta(z)\right\}. \tag{5}$$

Here n_0 is the average refractive index and Λ, $\Delta n(z)$, and $\theta(z)$ specify the grating parameters, i.e. reference period, grating chirp (local strength and phase variation) and local period. Simplest and first realized structures were gratings having a constant, positive-only refractive index change along the fiber axis, i.e. uniform gratings. These gratings, however, are not desirable in WDM applications because for a flat-top pass they have very strong side lobes on both sides of the reflection spectrum causing high crosstalk between the adjacent channels. These side lobes can be reduced by changing the index modulation along the fiber length, i.e. using a procedure called apodization. Gratings can be written by using different apodization profiles such as Gaussian and Blackman profiles. By a careful design and choice of apodization profile gratings having higher than 30 dB side-lobe suppression can be realized [38]. The resulting periodic refractive index variation can be extremely complex giving FBGs extra degrees of freedom in the design process compared to gratings that are processed for example on waveguide structures.

Although the spectral response of these gratings yields a rectangular amplitude response, so far, however, the use of conventionally apodized gratings has been limited by the phase response that has been entirely dependent on the apodization profile of the grating. There have been several studies suggesting that the performance of conventionally apodized FBGs is limited by the dispersive effects caused by the sharp edged amplitude response and that compared to thin film filters, cascaded FBGs suffer significant penalties from accumulated dispersion/dispersion-slope [36]-[40]. However, application of new design methods based on inverse-scattering design algorithms [52], in conjunction with advanced fiber Bragg grating writing techniques, allows grating devices with significantly reduced in-band dispersion and greatly

improved amplitude characteristics [55]. Using such techniques the filter amplitude response can be defined independently from its dispersion response. This should be contrasted with conventionally apodized gratings, where filter amplitude and dispersion characteristics are intertwined and entirely dependent on the apodization profile. [III]

4.2 Inverse-scattering design algorithms

Generally the design of fiber Bragg grating has been considered as a direct problem, where the reflection spectrum of grating is calculated from the grating structure. Although the solution to the problem can be found by using different mathematical analysis methods such as Fourier transforms [44] or Bloch modes and transfer matrix methods [45],[46], coupled-mode theory is often used to analyze the properties of the gratings [47]-[50]. The scattering equations in coupled-mode theory are written in terms of two counter propagating slowly varying amplitude fields, *u(z)*, forward propagating and *v(z)*, backward propagating fields that are related by coupled mode equations [54]

$$\begin{aligned} \frac{du(z)}{dz} &= -i\delta(z)u(z) + q(z)v(z) \\ \frac{dv(z)}{dz} &= i\delta(z)v(z) + q^*(z)u(z) \end{aligned} \tag{6}$$

where $q = q(z)$ is the grating coupling coefficient given by [54]

$$q(z) = \frac{-i\pi}{2n_0\Lambda}\Delta n(z)e^{-i\theta(z)}, \tag{7}$$

and $\delta(z)$ is the detuning parameter compared to the Bragg design wavenumber β_B

$$\delta = \beta - \beta_B = \frac{2\pi n_0}{\lambda} - \frac{\pi}{\Lambda}. \tag{8}$$

Boundary conditions of this particular scattering geometry are $u(0) = 1$ and $v(L) = 0$, where L is the total length of the grating. Equation (6) can be reduced into a single differential equation by introducing a local reflection coefficient $\rho(z,\delta)$ [54]

$$\rho = \frac{v(z,\delta)}{u(z,\delta)} \tag{9}$$

and by calculating $d\rho/dz$ and substituting du/dz and dv/dz from Eq. (6) [54]

$$\frac{d\rho}{dz} = 2i\delta(z)\rho(z) - q(z)\rho^2 + q^*(z) \tag{10}$$

This equation is also known as Riccati equation and can be numerically solved for reflection coefficient $r(\delta) = \rho(0,\delta)$ to obtain the spectral response of the desired grating. However, direct methods to find a solution to the equation are approximate and valid only for weak gratings [50]. These limitations can be avoided by using inverse scattering methods to design gratings.

Inverse problem (or synthesis) in terms of designing fiber Bragg gratings amounts to finding the grating structure, i.e. index modulation profile, from a given or desired spectral and temporal profile of grating [51],[52],[54]. The grating synthesis problem can be solved by inverse scattering techniques that can be divided broadly into three main categories: 1) Fourier transformation techniques also known as first-order Born approximation, where the problem reduces into finding an inverse Fourier transform of the reflection coefficient. This method is only valid for weak gratings (reflectivities

below 50 %) and is not reliable for the design of very complex filters. 2) Exact integral equation solutions. The main drawback of these methods is the difficulty to solve the integral equations. Integral equations can be solved by using Gelfand-Levitan-Marchenko (GLM) equations but the solutions have been limited to reflection coefficients that can be expressed as rational functions or alternatively the iteration methods required to solve GLM equations have been approximate or too time consuming. 3) Discrete inverse scattering methods that are based on layer peeling algorithms (discrete layer peeling, DLP) that exploit the physical properties and structure of the layered media. This method relies on causality arguments. The coupling coefficient at the front end of the gratings can be determined assuming that the grating is excited by a delta probe. Assumption is valid since in the beginning the light has no time to penetrate deeply into the grating and hence is affected only by the first layer. After knowing the coupling coefficient of the first layer the fields are propagated to the next layer of the grating by using transfer matrix method and the coupling coefficient can be determined again since the first layer has been peeled off. This process is continued until the entire grating structure is reconstructed.

Discrete inverse scattering method is based on discretization of the identified grating structure. Discrete model of a fiber grating is formed by a series of discrete reflectors (complex reflectors), T_ρ. and propagation matrices T_Δ in given by [51]-[54]

$$T_\rho = \left(1 - |\rho|^2\right)^{-1/2} \begin{bmatrix} 1 & -\rho^* \\ -\rho & 1 \end{bmatrix}. \tag{11}$$

$$T_\Delta = \begin{bmatrix} e^{i\delta\Delta} & 0 \\ 0 & e^{-i\delta\Delta} \end{bmatrix}, \tag{12}$$

where ρ is the discrete, complex reflection coefficient

$$\rho = -\tanh\left(|q|\Delta\right)\frac{q^*}{|q|}. \tag{13}$$

The entire discretized grating is thus a series of discrete reflectors with a distance Δ between each other. The approximation can be made exact by applying a suitable synthesis algorithm that includes the multiple reflections within the grating structure. Reflections can be f. ex. included in the algorithm by writing the solution to the coupled-wave difference equations in terms of path integrals that extend to all propagation paths with a given number of scattering events [52]. The target of the algorithm is to find a coupling function *q(z)* for an identified grating so that its spectral response (or impulse time response) matches to a given spectral and temporal profile within the desired degree. The design for the grating can be obtained by solving the synthesis problem recursively by using a layer-peeling algorithm [51], [52].

The characteristics of a grating designed by the inverse scattering layer peeling algorithm are compared to the conventional Blackman apodized grating in Fig. 14. The normalized refractive-index modulation profiles of the two grating types are shown in Fig. 14(a). The corresponding reflectivity and transmissivity spectra are shown in Fig. 14(b), while the resulting group-delay variations are shown in Fig. 14(c). As a result of using the inverse-scattering layer peeling design, the produced gratings show much lower in-band group-delay variations and much squarer reflectivity characteristics. [III]

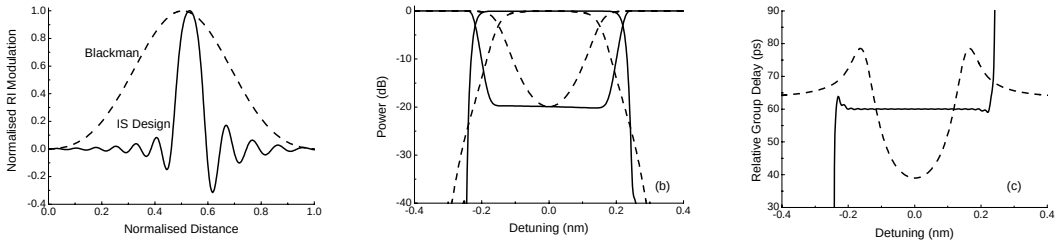

(a) (b) (c)

Figure 14. Physical and spectral characteristics of conventional Blackman-apodized gratings (dashed lines) and advanced inverse-scattered low-dispersion gratings (solid lines). (a) Normalized refractive index (RI) modulation profile against normalized grating length (b) Reflectivity and transmissivity spectra, and (c) group delay variations. [III]

4.3 Dispersion penalty of a cascade of linear-phase fiber Bragg grating

The experimental set-up to compare the in-band dispersion penalty of a cascade of linear-phase fiber Bragg grating (FBG) filters with conventional apodized FBG filters is shown in Fig. 15(a). In the measurements a tunable laser is externally modulated at 10 Gb/s with NRZ format that was pseudo-random bit stream (PRBS) 2^{31}-1 long. The signal is passed through a cascade of five gratings (operating in reflection mode) and a variable attenuator to a receiver and bit-error ratio (BER) tester. Experimental set-up to measure the additional penalty on a dropped channel caused by a cascade of five adjacent channel gratings is shown in Fig. 15(b). Here, before dropping the measured optical channel, signal is passed through five adjacent-channel FBG filters. [III]

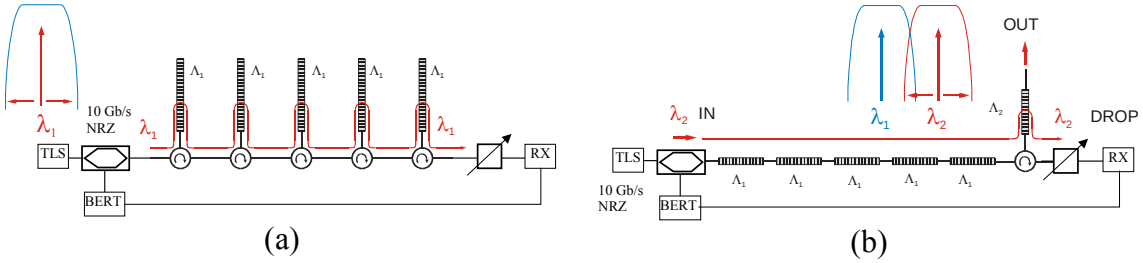

(a) (b)

Figure 15. (a) Experimental set-up for the power penalty measurements due to in-band dispersion/dispersion-slope of five FBG filters. (b) Set-up to measure the additional penalty on a dropped channel caused by a cascade of five adjacent-channel gratings. [III]

The time-delay spectrum of each FBG was measured using a standard modulation phase-shift technique utilizing a tunable laser and a network analyser [56]. The spectral characteristics and time-delay performance of a cascade of five FBGs operated in reflection mode are shown in Fig. 16(a). The time delay for linear-phase FBGs (solid line) remains nearly constant across the whole reflection band even after the cascade of five FBGs, whereas the time delay for conventional apodized FBGs (dashed line) increases considerably especially near the band edges. [III]

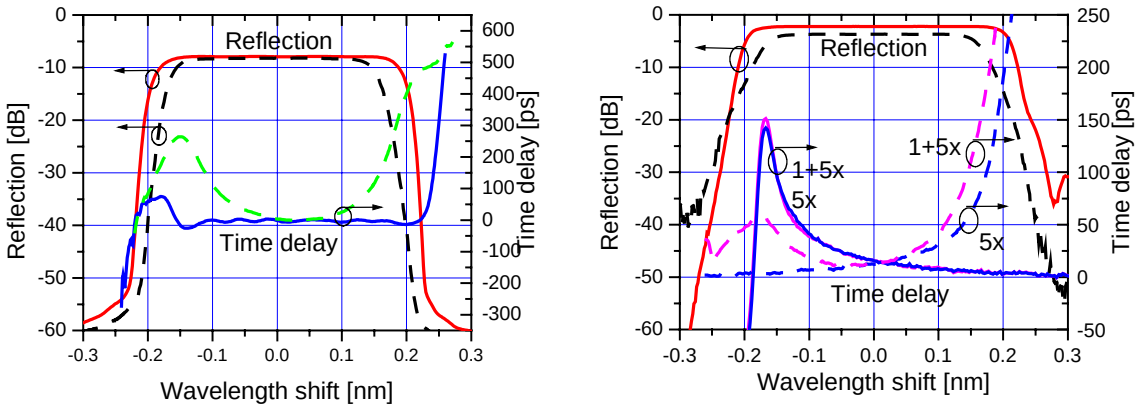

Figure 16. (a) Measured total reflectivity and time-delay spectra of five low-dispersion, linear-phase (solid line) and conventional fiber Bragg grating filters (dashed line) as shown in Fig. 15(a). (b) Measured total reflectivity and time-delay spectra of the cascade shown in Fig. 15(b) using linear-phase (solid line) and conventional fiber Bragg grating filters (dashed line). The total response consists of the accumulation of the out-of-band transmission through five identical gratings and the in-band reflection of a single grating.

Results of the accumulated time delay of the cascade shown in Fig. 15(b) are presented in Fig. 16(b). The total response consists of the accumulation of the out-of-band transmission through five identical gratings and the in-band reflection of a single grating. The single grating corresponds to the dropped channel (λ_2), while the five identical gratings correspond to the adjacent channel slot (λ_1). In the case of linear-phase (solid line), low dispersion gratings, the cascade of the five adjacent-channel FBGs were lying at shorter wavelength side ($\lambda_1<\lambda_2$) providing a slight tilt in time-delay response that corresponds to small negative (normal) dispersion. As can be seen from Fig. 16(b), the increase in total time-delay response is contributed entirely by the cascade of adjacent gratings. The center wavelength of the gratings inducing out-of-band dispersion in the cascade of conventional apodized gratings (dashed line), on the other hand, was lying on the long wavelength side ($\lambda_1>\lambda_2$) leading to positive (anomalous) dispersion. In this case, the time-delay slope and, therefore, the dispersion magnitude is much more pronounced. [III]

The power penalties due to the increased in-band and out-of-band dispersion/dispersion-slope in the cascades of FBGs, (shown in Figs. 15(a) and 15(b)), were measured as a function of transmitted signal (λ_2) detuning from the channel center wavelength. Figure 17(a) shows the power penalties induced by the accumulated in-band dispersion, after consecutive reflections by a cascade of five low-dispersion (or conventional) FBGs, as a function of the wavelength detuning from the channel center (see Fig. 15(a)). Figure 17(b), on the other hand, shows the power penalties induced by the accumulated dispersion, after propagating through a cascade of five low-dispersion (or conventional) *adjacent-channel* FBGs before reflecting at the drop grating, as a function of the wavelength detuning from the drop-channel center (see Fig. 15(b)). Results from the measurements are summarized in Table I.

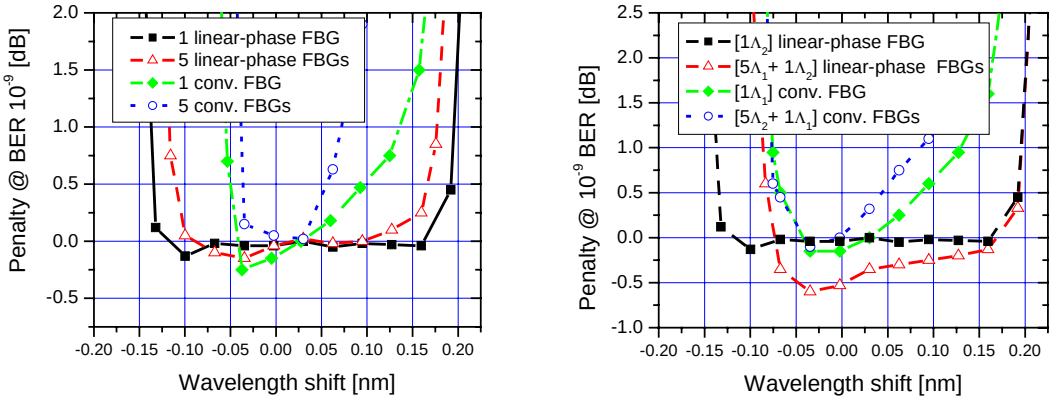

(a) (b)

Figure 17. (a) Power penalties induced by the accumulated in-band dispersion, after consecutive reflections by a cascade of five low-dispersion (or conventional) FBGs, as a function of the wavelength detuning from the channel center (see Fig. 15(a)). (b) Power penalties induced by the accumulated dispersion, after propagating through a cascade of five low-dispersion (or conventional) adjacent-channel FBGs before reflecting at the drop grating, as a function of the wavelength detuning from the drop-channel centre (see Fig. 15(b)). The single grating reflection penalties are also shown for comparison. Bit rate is 10 Gb/s and power penalty is measured at BER 10^{-9}. [III]

At the penalty level of 0.5 dB, the in-band bandwidth of a single conventional apodized FBG is 19 GHz and it is narrowed down to 11 GHz after the cascade of five gratings and down to 13 GHz in case of adjacent-channel FBGs. Power penalty results for linear-phase FBGs show twice as wide usable bandwidth for a single FBG (40 GHz) and more than three times wider bandwidth after the cascade of five FBGs (34 GHz). Thus, the usable bandwidth of linear-phase FBGs/FBG cascades is mainly limited by the reflectivity bandwidth whereas the usable bandwidth of conventional apodized FBGs/FBG cascades is severely limited by the dispersion near the band edges. Taking into account the results shown in Fig. 16(a) it can be deduced that the wider usable bandwidth of the case of linear-phase FBGs, as compared with the conventional ones, is predominantly due to the low in-band dispersion of the drop-channel grating. The penalty induced by the out-of-band accumulated dispersion for both types of gratings is comparable. The negative penalty (gain) at the short wavelength side of the linear-phase FBG cascade is a result of interaction of the transmitter positive chirp with the accumulated negative dispersion, which eventually compresses slightly the transmitted pulses [38].

The performance of the various types of gratings in WDM systems can be compared by introducing bandwidth utilisation (BU) factor defined as the ratio of the 0.5 dB power penalty bandwidth over the single-grating –0.5 dB reflectivity bandwidth. The closer to 100% the BU factors the better the grating quality. From Figs. 16(a) and 17(a), it is seen that the BU factor of a single linear-dispersion grating is 89%, while for the five-grating cascade is 76%. The corresponding factors for the conventional gratings are 53% and 31%.

Table I: Comparison of the 0.5 dB reflectivity bandwidth, 0.5dB power penalty bandwidth and BU factor of conventional, apodized FBGs and low-dispersion, linear-phase FBGs and FBG cascades. [III]

	Linear-phase FBG, in-band			Conventional, apodised FBG		
# of FBGs	0.5 dB reflection BW	0.5 dB penalty BW	BW utilization factor	0.5 dB reflection BW	0.5 dB penalty BW	BW utilization factor
1	45 GHz	40 GHz	89%	36 GHz	19 GHz	53%
5	40 GHz	34 GHz	76%	33 GHz	11 GHz	31%

5 High power DFB fiber lasers

The introduction of fiber Bragg gratings has greatly simplified the design and manufacturing of single-frequency lasers as short, monolithic in-fiber lasers, pumped by diode pumps can be built by direct UV-writing into the rare-earth doped fiber [57]-[63]. These fiber Bragg grating based distributed feedback fiber lasers (DFB FL) are attractive alternatives to semiconductor lasers due to their fabrication simplicity, low relative intensity noise and high wavelength accuracy and stability attributed by the temperature insensitive fiber gratings. They are especially attractive solutions to be used in ultradense WDM and CATV systems. There is also an increased interest in developing efficient single-frequency sources for eye-safe measurements and ranging, spectroscopy and frequency doubling.

Two types of fibers have been used in fabrication of DFB FLs: Er-doped germanosilicate fibers and Er:Yb-codoped phosphosilicate fibers. Earliest DFB FLs were based on Er-doped fibers with large amounts of germanium doped into the core to increase the photosensitivity of the fiber. Hence, strong Bragg gratings could be directly UV-written into the doped core. Er-doped DFB FL can be pumped either at 980 nm or 1480 and can lase at wavelengths from C-band to L-band (1530-1607 nm) [63]. The drawbacks of Er-doped DFB FLs are poor efficiency and low output power. Additionally, to obtain single-frequency operation short length of fiber with very high concentration of Er-doping is required. In heavily doped Er-fibers some Er^{3+}-ions may form clusters in which local concentration can be much higher than that of uniformly distributed Er^{3+}-ions. This will result in co-operative upconversion processes that decreases the efficiency and is also an origin to instabilities in the laser such as increased relative intensity noise and self-pulsing effects [64]-[68]. Er-doped DFB FLs are also very sensitive to the pump source perturbations. The absorption line of Er^{3+}-ions at 980 nm is very narrow and hence pump power fluctuations and wavelength shift arising from for example small back reflections (that are common in practical systems) can lead to low-frequency instability in the fiber lasers. This can be seen as output power fluctuations that can be detrimental to the WDM system performance.

The efficiency of the DFB FL can be increased by using Yb-codoped Er-fibers. Er:Yb-codoped fibers are designed such that the pump energy is mainly absorbed by Yb^{3+}-ions and then resonantly transferred to Er^{3+}-ions. Yb^{3+}-ions do not suffer from the clustering and quenching problems and therefore two orders of magnitude higher pump absorption can be achieved due to much higher concentration and larger absorption cross-section of Yb^{3+}-ions. At the same time Yb-codoping efficiently reduces the relative intensity noise and self-pulsing effects related to the clustering and quenching effects in heavily Er-doped fibers. Furthermore, the broad pump absorption band reduces the effect of pump power fluctuations on the intensity noise attributed to wavelength shift of the 980 nm single-mode pumps and also gives access to much wider range of pump wavelengths ranging from 900 nm up to 1070 nm.

Fiber Bragg grating in DFB FLs based on Er/Yb-doped fibers is generally written in a UV-sensitized B-Ge doped ring surrounding the core of the fiber [59] due to the lack of photosensitivity in the phosphosilicate host glass. There have been some demonstrations of gratings written directly into the core of Er/Yb-codoped fibers but these methods tend to suffer from the increased writing time and produce lower efficiency DFB FLs (higher cavity losses). By manufacturing DFB FL with a phase-shifted grating written in the photosensitive ring around the doped core output powers

exceeding 40 mW (pumped by a 980 nm Ti:Sapphire laser) and slope efficiencies over 20% have been demonstrated [62].

5.1 Characteristics of a stand-alone DFB FL

The measured slope efficiency of a stand-alone Er:Yb-codoped DFB FL is shown in Fig. 18. The pump source, p1, in the measurements was a high-power fiber-based 977-nm ASE-source (see Figs. 5-8 and Fig. 21). The net efficiency of 40-mW (+16 dBm) DFB FL is 11% as shown in Fig. 18. The efficiency of DFB FL is significantly reduced at output powers >20 mW due to the finite energy transfer rate from excited Yb^{3+}-ions to ground state Er^{3+}-ions. At low powers, however, the slope efficiency exceeds 20%. [IV]

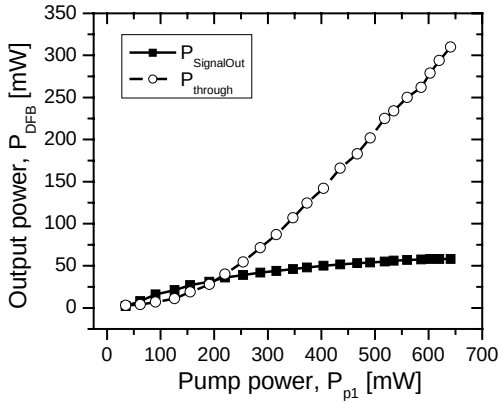

Figure 18. Output power and pump through of a DFB fiber laser pumped with a high-power ASE-source. Net efficiency to achieve 40 mW is 11%. [IV]

In CATV networks, the required RIN level for the transmitters is typically below 152 dB/Hz. However, in some systems using externally modulated transmitters even as low as –165 dB/Hz RIN levels are desired [72]. RIN characteristics of a stand-alone DFB FL are shown in Fig. 19. The measurement set-up is the same as in [69]. The level of the RIN of the DFB FL depends on the output power. The highest RIN value of –107 dB/Hz occurs at the frequency corresponding to the relaxation oscillation (RO) peak, which is situated around 300 kHz at the output power of 0 dBm. As pump power increases the laser becomes less noisy and the relaxation oscillation frequency is shifted towards higher frequencies. At the output power of +16 dBm, RIN at the RO frequency was as low as -131 dB/Hz ($f_{RO\ peak}$=1.34 MHz). At frequencies higher than 10 MHz, the RIN level below –160 dB/Hz is achieved. [IV]

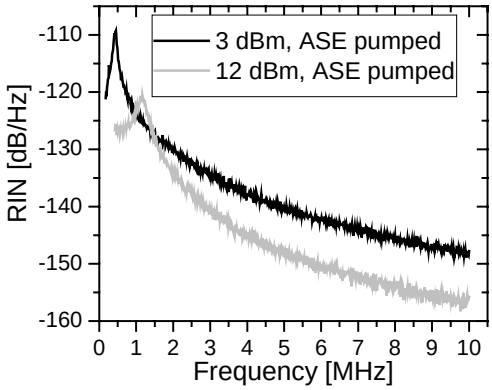

Figure 19. RIN of a stand-alone DFB FL pumped by an ASE-source at two different output powers. Resolution bandwidth: 10 kHz. [IV]

In high-density WDM and CATV systems, in addition to low RIN, other characteristics such as optical signal-to-noise (OSNR) and dispersion tolerance are important in the choice of transmitter. The OSNR of a stand-alone DFB FL is >60 dB as can be seen from the optical spectrum shown in Fig. 20(a). The importance of the high OSNR and dispersion tolerance were demonstrated in a transmission test in a 10 Gb/s NRZ system over 50 km of nonzero dispersion shifted fiber (NZ-DSF). Results from the experiment for three different type of transmitters are shown in Fig. 20(b). As can be seen, the performance of the external cavity tunable laser and DFB FL are slightly better mainly due to the higher side-mode suppression ratio [62].

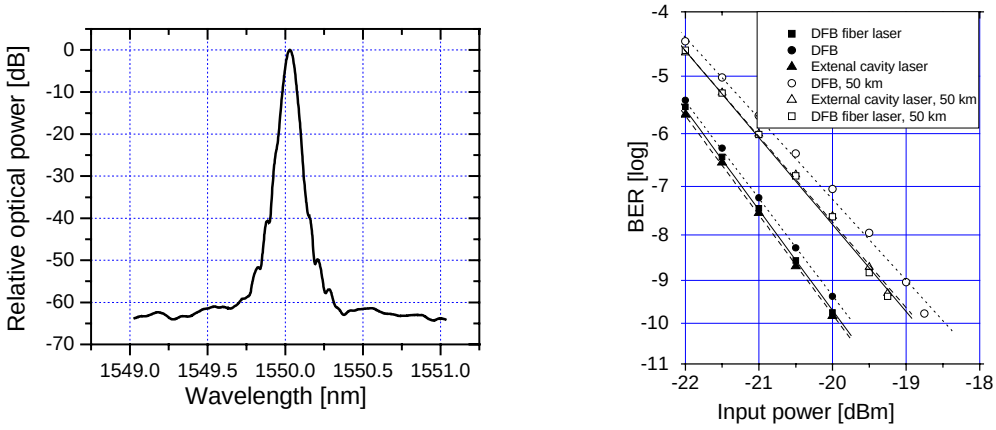

(a) (b)

Figure 20. (a) Optical signal-to-noise ratio of a stand-alone DFB FL. (b) Bit error rate performance of a stand-alone DFB FL compared to an external cavity semiconductor laser and DFB laser. Pseudorandom bit sequence used is 2^{31}-1 and bit rate 10 Gb/s [VI].

5.2 Performance of amplified DFB FLs

Despite the considerable improvement in the slope efficiency, high output powers (>40 mW required for CATV or >100 mW for high-resolution spectroscopy) directly from DFB FLs have not been easy to achieve due to short device length and low single-pass gain. Output power can be significantly increased by using a master-oscillator-and-power-amplifier (MOPA) configuration [70],[71]. With MOPA configuration (in this thesis referred as amplified DFB FL) the net efficiency and the output power of the DFB FL can be increased significantly. However, as the

efficiency and the output power of the DFB FL is improved other important characteristics affecting system performance such as OSNR and RIN are degraded. [IV]

5.2.1 Relative intensity noise

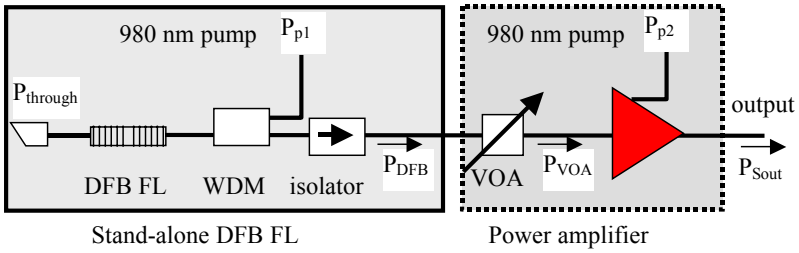

Figure 21. Experimental set-up to characterize stand-alone and amplified DFB FL. Variable optical attenuator (VOA) is used to simulate the loss element of a remotely located DFB FL. P_{p1}= optical power of the pump p1, P_{p2}= optical power of the pump p2, P_{DFB}= output power of the DFB FL, P_{VOA}=optical power after VOA, P_{Sout}= optical power of amplified DFB FL, $\eta_{DFB\ FL} = P_{DFB}/P_{p1}$, $\eta_{amplified\ DFB\ FL} = P_{Sout}/(P_{p1}+P_{p2})$. [IV]

The experimental set-up to compare the characteristics of a stand-alone and an amplified DFB FL in the measurements is shown in Fig. 21. The output power of the stand-alone DFB FL was shown in Fig. 18, which also showed the residual pump power leaking through the DFB FL. It is clearly seen that enough pump power is available to efficiently pump the power amplifier of the amplified DFB FL. The comparison of the RIN of a stand-alone DFB FL and an amplified DFB FL at three different frequencies (RO frequency, 5 MHz and 50 MHz) is shown in Fig. 22. The power amplifier in the measurements was a conventional core-pumped EDFA (40 mW of output power). Input power to the power amplifier was changed from 0 dBm to +12 dBm. At frequencies below 5 MHz, RIN follows closely the RIN of a stand-alone DFB FL at the same output power, as was the input power to the power amplifier. At frequencies above 20 MHz the amplified DFB FL has a higher level of RIN. RIN values below –160 dB/Hz at >50 MHz can be achieved by having input power >+15 dBm to the cladding-pumped power amplifier. [IV]

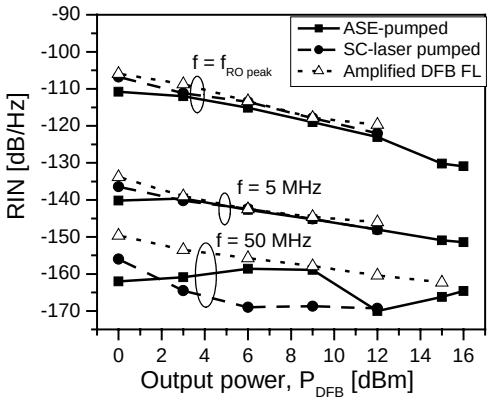

Figure 22. Comparison of a DFB fiber laser pumped with a fiber-based ASE-source and semiconductor (SC) pump. Also shown in the figure is the RIN of an amplified DFB FL. RIN values are measured at the relaxation oscillation frequency, f=5 MHz and f=50 MHz. Resolution bandwidth: 10 kHz. [IV]

5.2.2 Optical signal-to-noise ratio

Optical signal-to-noise ratio (OSNR) of the DFB FL was measured with an optical spectrum analyzer with 0.06 nm spectral resolution. As was shown in Fig. 20(a) DFB FL at an output power of +16 dBm has an OSNR of 63 dB whereas amplified DFB FL with the same output power has significantly lower OSNR depending on the input power to the power amplifier. Degradation of OSNR was analyzed in two cases: (i) DFB FL is directly followed by the power amplifier and (ii) there is a significant loss element between the laser and the power amplifier. The latter situation may occur when the laser source and a modulator are situated at different locations [73],[74]. In such application the output power of the DFB FL has to be maintained at a relatively low level in order to prevent stimulated Brillouin scattering. In the measurements, the output power from the DFB FL was 0 dBm and the loss generated by the fiber was simulated by an attenuator as shown in Fig. 21. The OSNR as a function of the input power to the power amplifier is shown in Fig. 23. In the measurements the input power to the power amplifier was varied whereas the output power from the power amplifier was adjusted to a constant power level of 40 mW by changing the pump power to the power amplifier. With input powers ranging from -15 dBm to +12 dBm, OSNR increases from 40 dB to 59 dB, thus outperforming the 30-dB minimum OSNR of a commercially available high-power DFB laser. The total pump power required to achieve 40 mW of output power varies from 180 mW to 260 mW. Figure 23 also shows that, OSNR values better than 60 dB can be accomplished by increasing the input power to the 1-W output power amplifier over +15 dBm. [IV]

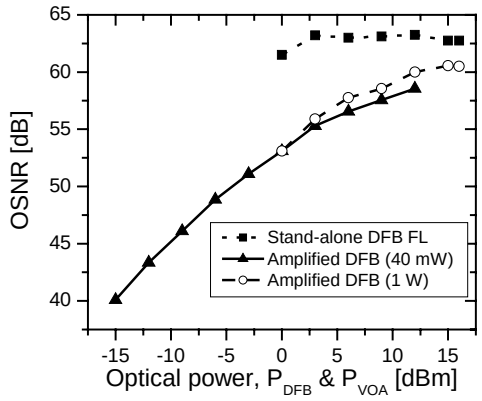

Figure 23. Optical signal-to-noise ratio (OSNR) as a function of input power to the power amplifier. The output power of amplified DFB FL using a core-pumped power amplifier was +16 dBm (40 mW). The output power of the amplified DFB FL with cladding-pumped power amplifier was +30 dBm (1 W). [IV]

5.2.3 Increased efficiency with degraded performance

Performance trade-offs in terms of RIN and OSNR of an amplified DFB FL with the output power of 40 mW compared to stand-alone DFB FL as a function of improved net efficiency ($\eta_{\text{amplified DFB FL}}/\eta_{\text{DFB FL}}$) are illustrated in Fig. 24. The stand-alone 40-mW DFB FL had an OSNR of 63 dB and RIN at relaxation RO frequency of –131 dB/Hz and at 5 MHz of -152 dB/Hz. The net efficiency of the laser was 11%. Figure 24 shows that an amplified DFB FL can be twice as efficient (net efficiency=22%) as a stand-alone DFB FL. At the same time, however, OSNR is degraded by 10 dB and RIN at RO frequency is increased by 25 dB and by 18 dB at 5 MHz. The degradation

of the RIN of the amplified DFB FL is dependent on the output power of the DFB FL, i.e. master oscillator, preceding the power amplifier. As the power of the master-oscillator is increased the degradation of the RIN level is decreased. The reduced OSNR is caused by ASE noise. The best compromise in terms of improved efficiency (efficiency improvement 77%, net efficiency 20%) and degraded RIN and OSNR, is to use a +6-dBm DFB FL as a master-oscillator. In this case the degradation of OSNR is 6.5 dB and RIN at 5 MHz 9 dB. The total pump power used to achieve 40 mW of output power in this case is 200 mW. The efficiency of the EDFA used in the measurements was 32%. As the efficiency of the Er^{3+}-fibre used in the amplifier is 37% source efficiencies of about 25% can be achieved with an improved amplifier design. [IV]

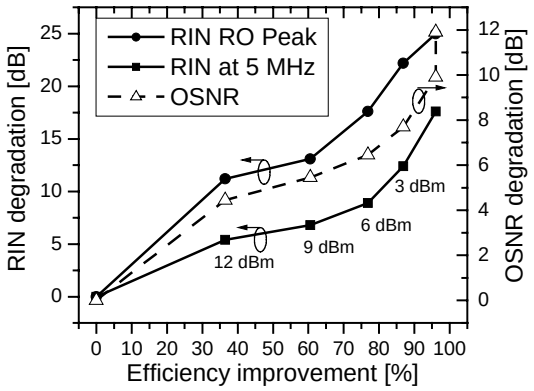

Figure 24. Performance degradation of the amplified DFB FL as a function of improved net efficiency ($\eta_{\text{amplified DFB FL}}/\eta_{\text{DFB FL}}$) compared to the performance of a 16-dBm stand-alone DFB FL ($RIN_{\text{RO Peak}}$=-131 dB/Hz, $RIN_{\text{at 5 MHz}}$=-152 dB/Hz, OSNR=63 dB, net efficiency=11%). [IV]

5.2.4 Stimulated Brillouin scattering

One of the major limitations set-forth to a narrow linewidth, high-power amplified DFB FL is stimulated Brillouin scattering (SBS), which limits the launched power from the source. In non-return-to-zero (NRZ) optical transmission systems, SBS threshold can be increased either by the use of transmitters with inherently broader linewidth or by means of external frequency dithering or phase modulation. In applications, where an unmodulated narrow linewidth source is used (such as spectroscopy and frequency doubling) SBS can be suppressed by choosing the gain medium of the power amplifier so that the SBS threshold is increased. This can be achieved by shortening the length of the amplifying media and/or by adjusting the diameter of the doped core [76].

The limitations of the launch power due to SBS of a modulated laser source were studied with a measurement set-up similar to [75]. In the experiments three different type of transmitters were compared: DFB FL (linewidth 50 kHz), external cavity tunable laser (linewidth 1 MHz) and semiconductor DFB laser (linewidth 10 MHz). Transmitters were externally modulated at 10 Gb/s pseudorandom bit sequence of 2^{31}-1 and launched into 50 km of NZ-DSF. In the measurements, the backwards-scattered optical power was measured with an optical spectrum analyzer. SBS threshold was determined to be a point, where the Brillouin backscattered power was 10 dB lower than the Rayleigh backscattered signal power. The measured thresholds were 4.2 dBm for both DFB fiber laser and external cavity tunable laser and 5.7 dBm for semiconductor DFB laser as shown in Fig. 25(a). [VI]

Transmitter	Linewidth	SBS threshold
DFB fiber laser	50 kHz	4.2 dBm
External cavity laser	1 MHz	4.2 dBm
Semiconductor DFB laser	10 MHz	5.7 dBm

(a)

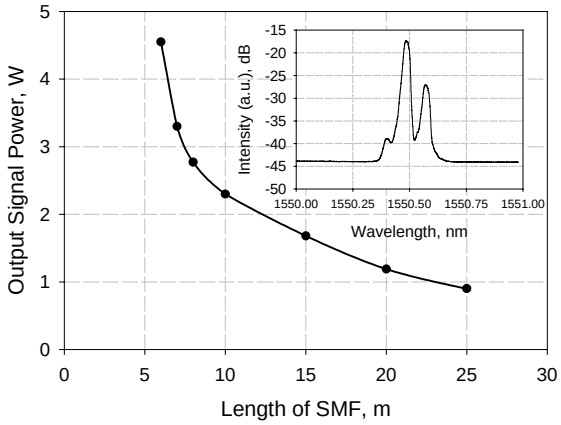

(b)

Figure 25. (a) Stimulated Brillouin thresholds of DFB fiber laser, external cavity tuneable semiconductor laser and semiconductor DFB-laser in 10 Gb/s NRZ transmission experiment [VI]. (b) Variation of SBS threshold as a function of SMF length added at the output of MOPA. Inset shows the optical spectrum while SBS reaches its threshold.

The measurement results of the variation of SBS threshold power on the fiber length of a narrow linewidth unmodulated amplified DFB FL in high signal power regime are shown 25(b). In the MOPA for power range from 1 W to 10 W, a DFB FL with output power of 10 mW and a GTWave fiber assembly containing two pump fibers and one Er:Yb co-doped signal fiber (core diameter 8 μm, NA=0.12) was used. The outer diameter of the fibers was 80 μm. The impact of SBS is minimized by having a high absorption coefficient of the doped core (~200 dB/m @915 nm) allowing the use of only 10 m long gain medium. Fig. 25(b) plots the exponential dependence of SBS threshold power on the length of single mode fiber (SMF) added to the MOPA. This shows that by keeping the output pigtail of the fiber laser short, output powers in excess of 10 W can be achieved by scaling up the pump power. Further improvement can be achieved by shortening the length of the amplifying gain medium with 975 nm pumping or by increasing the diameter of the doped core.

6 Scalability of metropolitan WDM networks

Metropolitan area networks (MAN) aggregate various traffic types originating in the access networks and transmit the information either within the same geographical area or to remote locations through egress nodes interfacing the access networks and a backbone network [77]. In MAN the major driving force determining the design of the network is cost. This originates from the much smaller customer base sharing the capital and operating expenditures compared to the backbone networks. Additional difficulty in designing metropolitan area networks (MAN) is the dynamic nature of the data traffic due to the customer requirements for individual traffic streams with highly variable attendant characteristics. WDM technology has several advantages over its competing counterparts to meet these demands such as large bandwidth, high degree of configurability and transparency to different data transmission protocols. The main obstacle, however, to hinder the penetration of WDM technology in metropolitan areas is cost. Therefore, the design of transparent WDM metropolitan networks requires careful engineering and the use of optimised optical layer components and fiber.

One of the important features of metro networks is that the ratio of network nodes per transmission distance is substantially higher than that in long-haul transmission [80]. Hence the node losses could dominate over the transmission losses in the fibers. This not only increases the network cost (the losses caused by the nodes have to be compensated by optical amplifiers at extra cost) but also imposes specific requirements for the components used in metropolitan optical networks. Other impairments that limit the size of the network are noise accumulation, optical power divergence of the different channels, fiber and component chromatic dispersion, laser frequency chirp, linear crosstalk, filter concatenation and fiber nonlinearities. To ensure scalable network architectures, network designers need to carefully analyze the effect of different impairments on the signal path through numerous optical elements and develop network architectures taking advantage of low-cost optical technologies. In these networks, the need for amplification is minimized and the reliability of the network is maximized by the use of simple nodes that are built up from a few low-cost, passive, static devices [V].

6.1 Metropolitan Bi-directional Multifiber WDM-Ring Network

6.1.1 Network architecture

Multifiber WDM-ring networks using bi-directional transmission provide a reliable and a cost-effective means to enhance the capacity of the metropolitan area networks (MAN). Multifiber WDM-ring networks combine the benefits of space-division-multiplexing and WDM techniques to achieve high bandwidth inexpensively [81]-[83]. With the help of multiple fibers the number of wavelengths in a single fiber can be kept moderately low. This lowers the bypass losses and enables simple node structure that is necessary in minimizing the need for optical amplification in the MAN. Resource sharing and reliability of the network can be improved further by implementing bi-directional WDM transmission in each of the fiber rings [84]-[90], [V].

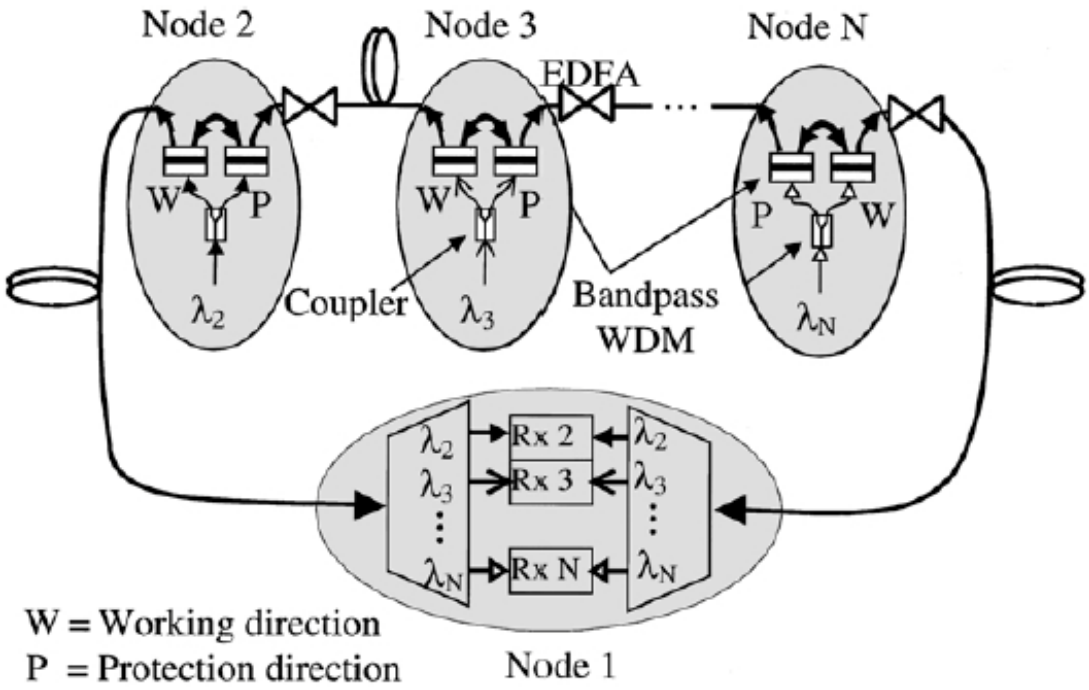

Figure 26. A bi-directional fiber ring, which is the building block of a multifiber WDM-ring network. [V]

The basic building structure of the multifiber WDM-ring network is a single fiber ring shown in Fig. 26. Transmission in each of the fiber rings is bi-directional and the link is terminated at both ends by demultiplexers and receivers. The network is built up from multiple fiber rings as shown in Fig. 27. The number of fiber rings in the connecting cable equals the number of nodes in the network. Each node receives signals from a fiber ring dedicated to it while transmitting signals to the other fiber rings. To simplify the wavelength assignment, each node transmits at wavelengths not covered by the other nodes in the network. Bypass losses of the ring are low because the addition of signals in the transmitting nodes is performed by bandpass WDMs that can be f. ex highly cascadable linear phase fiber Bragg gratings. This reduces the need for optical amplification in the network and enables the use of low gain, shared-pump EDFAs or distributed Raman amplification. The employment of only a few low-gain EDFAs in the network is also beneficial in hindering the build-up of RIN due to multiple reflections and coherent crosstalk. [V]

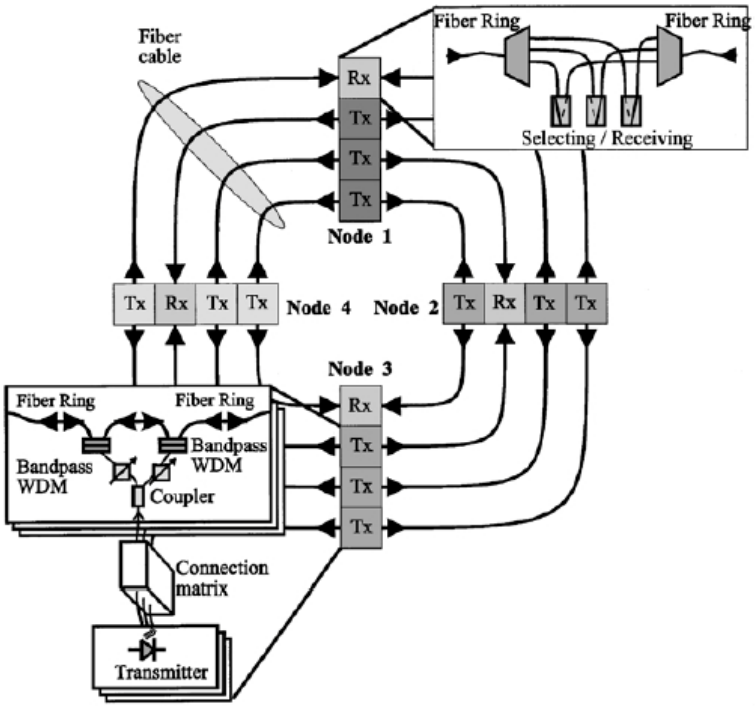

Figure 27. The network architecture and the node configuration of the multifiber WDM-ring network with four nodes and four fibers. Transmission in the fibers is bi-directional. Tx=transmitter and Rx=receiver. [V]

To provide low-cost bi-directional amplification for multifiber rings, shared-pump EDFAs are implemented in the network. The cost of the shared-pump amplifiers reduced by sharing the pump source [see Fig. 5] and control electronics between the amplifiers for different fibers at the same position in the multifiber ring. The idea of this type of EDFAs is to divide the overall gain needed to compensate the losses between several low-gain amplifiers (~10-15 dB). By keeping the gain of individual amplifiers low, the build-up of relative intensity noise (RIN) due to Rayleigh backscattering is reduced and isolators are not needed. [V]

6.1.2 Double Rayleigh backscattering in optical amplified bi-directional transmission systems

In optical transmission systems, even if all discrete reflection points are eliminated, multiple reflection noise is still generated due to double Rayleigh backscattering in the fiber [91]-[95]. In optically amplified bi-directional systems, where the amplifier lies between two scattering sites, the effect of RIN arising from multiple reflections and Rayleigh backscattering is increased because the scattered signal is twice amplified. This can severely degrade the performance of the system. The build-up of Rayleigh backscattering in an optically amplified transmission system is schematically illustrated in Figs. 28(a) and 28(b). In Fig. 28(a), the transmission system consists of a transmitter, 140 kilometers of fiber, an EDFA with 20-dB gain, and a receiver. On both sides of the amplifier multiple reflection noise is generated due to single and double Rayleigh backscattering. This reflection noise is further amplified by the EDFA, thus limiting the performance of the system. [V]

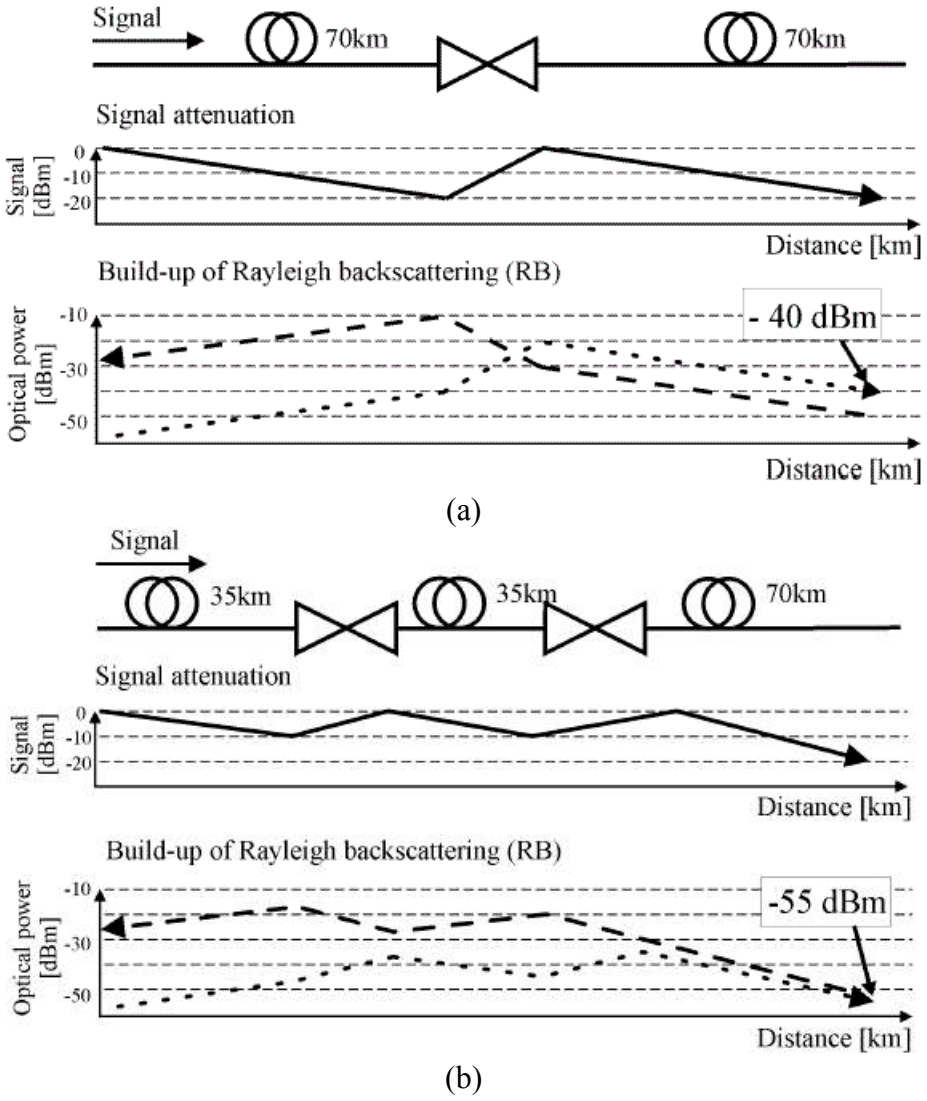

Figure 28. The signal attenuation and the build-up of Rayleigh scattering in a bi-directional fiber link with (a) one 20-dB amplifier and (b) with two separate 10-dB amplifiers. Dashed line indicates single and dotted line double Rayleigh backscattered signals. [V]

In high-speed systems, this type of reflection noise due to multiple Rayleigh backscattered signal limits the maximum EDFA gain to less than 20 dB [93]. To diminish the deterioration of the signal caused by this effect, the gain of the EDFA can be divided between two EDFAs. Fig. 28(b) shows a schematic picture of the build-up of Rayleigh backscattering in a fiber link with two low-gain amplifiers. With one 20-dB amplifier, the double Rayleigh backscattered light at the end of the transmission line is about 20 dB below the signal level (P_{DRB}= -40 dBm). As the gain is divided between two 10-dB amplifiers and the first fiber span is split into two 35-km parts, the aggregated Rayleigh backscattering is reduced. This type of arrangement reduces the level of Rayleigh backscattered light, traveling in the same direction as the signal, by 15 dB (P_{DRB}= -55 dBm). In these calculations, the difference between Rayleigh backscattering and signal power was assumed to be -30 dB, which is a typical value for standard telecom transmission fibers. [V]

The effect of RIN arising from Rayleigh backscattering can further be reduced by using directly modulated DFB-lasers in WDM systems employing bi-directional transmission. This is due to the frequency chirping of directly modulated DFB-lasers,

which broadens their optical spectrum. As the optical spectrum of the DFB-laser is broadened, a larger part of the noise originating from signal beating with the Rayleigh backscattered signal, falls out of the electrical bandwidth of the receiver [96]-[98]. [V]

6.1.3 Scalability results

The scalability of a metropolitan bi-directional multifiber wavelength-division-multiplexed (WDM) ring network was analyzed by using a bi-directional transmission model, which includes the major limiting factors in WDM-ring networks such as relative intensity noise (RIN) due to multiple Rayleigh backscattering, amplified spontaneous emission (ASE) accumulation in a cascade of bi-directional erbium-doped fiber amplifiers (EDFA), tilting of the EDFA gain spectrum. The scalability of the system was studied by varying three different attributes of the EDFA: 1) the gain of the EDFA, 2) the gain shaping of the EDFA and 3) the input saturation power of the EDFAs. The amplifiers having a gain of 8, 10, 12, 14, 17 or 20 dB were placed in the network nodes. The length of the fiber span and the number of nodes between successive EDFAs were set to have the total loss equal to the gain of the EDFA at 1540 nm. The gain curve of the EDFA corresponded to the measured gain curve of an EDFA with the gain of 12 dB at 1540 nm. The accepted power penalty of the worst channel in the network was below 1 dB at the BER of 10^{-9}. The channel spacing was 100 GHz and the bit rate 2.5 Gb/s. The parameters of the WDM components corresponded to the worst-case values given by the manufactures. [V]

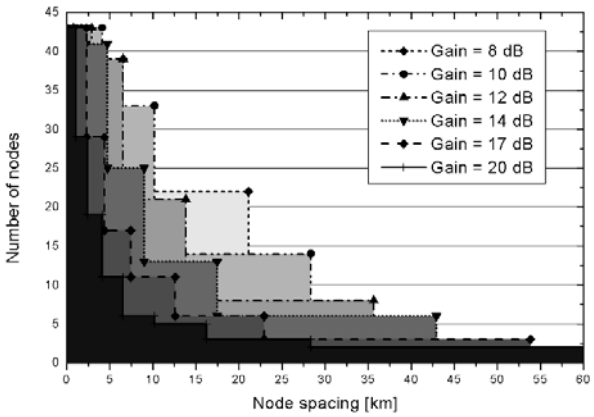

Figure 29. The effect of the EDFA gain on the scalability of the network. Input saturation power of the amplifiers was 3 dBm and gain tilt was 0.5 dB from 1530 to 1565 nm.

The maximum size of the network in metropolitan areas (node spacing 5-10 km) can be achieved by using EDFAs with a gain of 10-14 dB as shown in Fig. 29. The effect of RIN due to Rayleigh backscattering can be seen as asymptotic behaviour of the node number as the gain of the amplifiers is increased. With high gain amplifiers (G>14 dB) the size of the network with large node spacing decreases rapidly, indicating that the Rayleigh backscattering limits the scalability of the network. However, if the node spacing is short the scalability restriction imposed by the gain of the amplifiers is relaxed. [V]

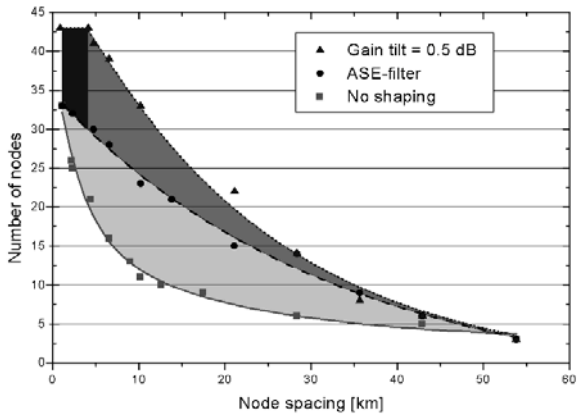

Figure 30. The maximum size of the network as a function of node spacing with three different gain shaping schemes. The input saturation power of the EDFAs was 3 dBm. Solid, dashed and dotted curves have been fitted to the points in the figure. Light gray area between dashed and solid curves is the scalability limit imposed by ASE-accumulation. Darker area between dashed and dotted curve illustrates the effect of gain tilt on the size of the network. Darkest area is the scalability limit imposed by the finite width of the EDFA gain spectrum. [V]

The effect of gain shaping and ASE-filtering of the EDFA on the scalability of the studied bi-directional system is illustrated in Fig. 30. The points in the figure correspond to the maximum size of the network when EDFAs with a gain of 8, 10, 12, 14, 17 or 20-dB were used. The step-like behaviour, similar to Fig. 29, is omitted for clarity. The number of channels in the network was equal to the node number and the input saturation point of the EDFAs was 3 dBm. Three different cases were simulated: 1) The gain curve of the EDFAs was not shaped at all, 2) only the ASE-peak was filtered out, or 3) the gain tilt was suppressed to 0.5 dB from 1530 nm to 1565 nm with a gain-flattening filter. [V]

Figure 30 indicates that shaping of the EDFA gain curve has a major effect on the scalability of a bi-directional transmission system. The light gray area between the dashed and solid curves indicates the scalability limit imposed by ASE-accumulation. ASE-accumulation is the major limiter of the network scalability when the node spacing is between 10-30 km. The darker area between gain-flattened and ASE-filtered curves illustrates the effect of gain tilt on the size of the network. Gain tilt is the main limiter of the scalability in the metropolitan area, i.e. when the node spacing is 5-10 km. This can be seen as a deviation of the ASE-filtered from the gain flattened curve below 25-km node spacing. The finite width of the EDFA gain spectrum (darkest area in the figure) limits the scalability when the node spacing is shorter than 5 km. The effect of Rayleigh scattering on the size of the network can also be seen from Fig. 30. At longer node spacing values, the width of the shaded areas decreases indicating that the RIN due to Rayleigh backscattering limits the scalability. [V]

6.2 High-density metropolitan WDM ring network

The circumference of metropolitan WDM ring networks can be as high as 600 km [78]. For this type of networks operating at bit rates of 10 Gb/s, chromatic dispersion is one of the main impairment limiting the scalability of the network. Dispersion penalty can be decreased and scalability of the WDM networks improved by implementing dispersion compensators in network but this would increase the cost of the network and complicate the network design. Hence, fiber manufactures are

promoting nonzero dispersion-shifted fiber (NZ-DSF) to be used in the next generation metropolitan area networks.

While NZ-DSFs simplify the dispersion compensation schemes in the transmission systems, there are conflicting needs to improve the spectral efficiency (i.e. decrease channel spacing) and to extend the span length between successive optical amplifiers in the metropolitan networks. The origins of the conflict are the lower thresholds for stimulated Brillouin scattering and four-wave mixing in high density metropolitan WDM networks (channel spacing 25 GHz) using NZ-DSF [99], [100]. Therefore the conventional methods to increase the length of the repeaterless sections such as increasing the output power of the transmitters and amplifiers and decreasing the fiber loss are not sufficient enough. Also the wavelength accuracy of the temperature controlled laser diodes is not sufficient to meet the strict wavelength stability requirements and external methods based on f.ex. multiwavelength meters and Fabry-Perot interferometers are required increasing the cost of the transmitters. Therefore the choice of the transmitter in these type of networks needs to be considered in combination with the amplification schemes and node structures so that the length of the repeaterless sections is maximized and the signal distortions due to fiber nonlinearities are minimized.

The three most important nonlinearities limiting the input powers launched to the fibers in high-density WDM systems are stimulated Brillouin scattering (SBS), four-wave mixing (FWM) and cross-phase modulation (XPM). Stimulated Brillouin scattering is an interaction of optical waves with sound waves in the fiber converting the input light into longer wavelength, backward-travelling Stokes light. The SBS threshold strongly depends on the source linewidth and therefore limits launched power of a single channel from a narrow linewidth source [101]-[107].

Four-wave mixing is an effect where two or more optical signals at different wavelengths mix together producing new co-propagating optical signals, sidebands, at different wavelengths. Generation of these sidebands degrades the performance of the WDM systems through crosstalk and excess attenuation. The efficiency of four-wave mixing depends on the channel spacing and the fiber dispersion. With low dispersion fibers such as NZ-DSF, the efficiency is higher due to the better phase matching conditions. With dense channel spacing FWM is a major limiter of the length of the repeaterless sections in high-density WDM systems based on NZ-DSF.

Cross-phase modulation (XPM) is a nonlinear phenomenon in which the phase of the optical signal is modulated by the intensity modulation of its neighboring signals [99]. XPM is converted into intensity distortions through group velocity dispersion. XPM limits the length of the repeaterless sections especially in systems with large channel number. Compared to FWM the signal distortions are not as profound since the influence of FWM quadruples when halving the channel spacing while signal distortions due to XPM are approximately inversely proportional to channel spacing [110]. Furthermore, signal distortions due to XPM can be reduced by choosing appropriate dispersion compensation scheme whereas FWM remains unchanged. XPM.

6.2.1 Increasing the length of repeaterless sections

Conventionally, SBS threshold can be increased either by the use of transmitters with inherently broader linewidth or by means of external frequency dithering or phase modulation. In high-density metropolitan networks, the choice of laser is preferred over other means to increase SBS threshold, because as the channel spacing is

decreased frequency dithered signal is destroyed by four-wave mixing (FWM) while the phase modulation increases the cost of the transmitters. The threshold for FWM can be increased with unequally spaced channels [108] or with the arrangement of orthogonal polarized signals [109]. These schemes, however, increase the cost of the network and complicate the network design and scalability. Unequally spaced channels scheme requires complex allocation of wavelengths and orthogonally polarized sig'nals scheme needs costly monitoring and control of the polarization state of the add/drop channels. [VI]

To increase the dynamic range without implementing additional EDFAs in the network nodes either the channel launch power has to be increased in conjunction with the reduction of the number of FWM products or transmission loss has to be compensated (fully or partially) by distributed optical amplification, e.g. Raman amplification. Number of FWM products can be decreased by using alternate channel spacing (i.e. removing every third channel). With this method, there is no additional design and manufacturing costs and at the same time the spectral efficiency of the network is reduced. [VI]

In this thesis three schemes to increase the length of the repeaterless sections were studied: transmitters with different spectral linewidth, distributed Raman amplification (DRA) and alternate channel allocation scheme. The experimental set-up to study limitations imposed by SBS and FWM in high-density metropolitan WDM networks is shown in Fig. 31. The transmission fiber used in all the experiments was NZ-DSF with effective area of 55 μm^2, zero dispersion wavelength at 1460 nm and dispersion of 4.5 ps/(nm·km). Three transmitters were operating at 10 Gb/s and the channel spacing was 25 GHz. The wavelengths of the channels were 1551.521, 1551.721 and 1551.921 nm. The transmitted signal was a NRZ pseudo-random bit stream with 2^{31}–1 pattern length. The total transmission distance in the experiment was 100 km. Three add/drop nodes and a dispersion compensating grating acting as a waveband router was placed in the system. Nodes consist of passive and fixed components (FBGs, circulators and isolators) having low loss both for the add/drop and express channels. The choice of low-dispersion and wide usable-bandwidth FBGs in the nodes allows the use of highly dense channel spacing in the network thus providing a highly scalable network architecture and also enabling optical broadcasting. To create worst-case nonlinear interaction conditions all the wavelengths are broadcasted through the networks nodes and no decorrelation fiber is used [100]. Variable attenuators in the nodes were used to adjust the launch power of the added channels to the levels of the express channels. Add/drop multiplexers were complemented with broadband fused WDM couplers to by-pass the Raman pump. [VI]

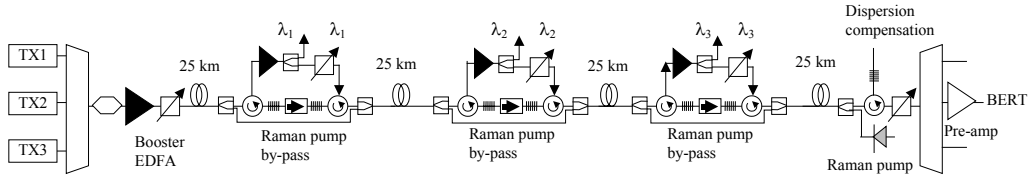

Figure 31. Experimental set-up to study limitations imposed by SBS and FWM in high-density metropolitan WDM networks. [VI]

In the experiments, the performance of three different type of transmitters was compared: DFB fiber laser (linewidth 50 kHz), external cavity tunable laser

(linewidth 1 MHz) and semiconductor DFB laser (linewidth 10 MHz). The SBS threshold and the BER performance of the transmitters are shown in Figs. 20(b) and 25(a), respectively.

To show the usefulness of DRA in metropolitan networks, we performed a 100-km transmission experiment with both three (channels 2-4) and five 25-GHz spaced channels (1551.321, 1551.521, 1551.721, 1551.921 and 1552.121 nm) operating at 10 Gb/s without any add/drop nodes along the transmission span. Polarization of the channels was aligned to same polarization state and no decorrelation fiber was used in order to achieve maximum strength of FWM. The channel launch power was varied from –4 to 2 dBm. The performance of the middle channel (1551.721 nm) suffering from the maximum amount of FWM crosstalk was analyzed and the results are shown in Fig. 32. In the case of using only a booster EDFA, the channel performance was acceptable (1 dB penalty at BER below 10^{-9}) with optical launch powers per channel from -4 dBm to 0 dBm/2 dBm (5 chs/3 chs), giving only a 4 dB/6 dB dynamic range and showing that the threshold for FWM mixing (0 dBm) is lower than the SBS threshold (4.2 dBm). As the channel count is increased, the maximum channel launch power is decreased even further thus reducing the dynamic range. Hence narrow linewidth sources with good inherent wavelength stability such as DFB FLs are suitable for high-density WDM networks as SBS is not the major limiting nonlinearity. [VI]

Limitations imposed by four wave mixing and OSNR	
Amplification scheme	Input power range
EDFA (3 ch/5 ch)	6 dB/4 dB
EDFA, Alternate channel spacing (3 ch/5 ch)	12 dB/ 8 dB
DRA (3 ch/5 ch)	13 dB/ 11 dB
DRA and alternate channel spacing (3 ch/5 ch)	19 dB/ 15 dB

Figure 32. The range of channel-launch powers in a high density WDM network. Maximum channel launch power is limited by four-wave mixing and the minimum launch-power limit is limited by OSNR. Transmission distance is 100 km. Pseudorandom bit sequence used is 2^{31}-1 and bit rate 10 Gb/s. Distributed Raman amplification (DRA) gain is 7 dB.

Alternate channel allocation scheme was evaluated by alternating with 25 GHz and 50 GHz channel spacing between successive channels. This resulted in an increase of the range of the channel-launch powers from 4 dB/6 dB to 8 dB/12 dB (5 ch/3 ch) as shown in Fig. 32. As the channel count is changed from three to five the increase of the dynamic range due to alternate channel scheme is reduced, as the number of FWM mixing products at the monitor wavelength is larger. Thus even at low channel counts (5 channels) DRA is the most efficient way to lengthen repeaterless sections and at larger channel counts the only practical way to increase the dynamic range. With 350 mW of pump power at 1480 nm (7 dB gain at 1551.721 nm) the dynamic range could be increased by 7 dB. [VI]

7 Summary

In this thesis new and improved in-fiber components for optical networks were introduced. These components are needed not only to cope with the future growth in traffic but also to bring down the size and cost of the transmission equipment. New measurement methods and measures to evaluate the component performance in the network environment were developed. Furthermore the importance of the components in improving the performance and the scalability of the optical networks were quantified in simulations and experimental network set-ups.

Two new practical, fiber coupled configurations of stable high-power cladding-pumped Yb-doped fiber sources operating at 977 nm were presented: a fiber laser and an ASE (amplified spontaneous emission) or superfluorescent source. Sources are based on an Yb-doped jacketed air-clad fiber and high brightness pumping. These fiber sources can reduce the cost of amplifiers by sharing the pump power between several EDFAs (shared-pump EDFAs) and by reducing the number of pumps in a single amplifier. The fiber sources can also be used to pump several DFB fiber lasers and therefore reduce the cost of optical transmitters.

The cost of optical amplification can also be brought down by broadening the amplification bandwidth and developing amplifiers that on their own offer a range of attractive features improving the performance of the transmission systems. The L-band EDFA based on GTWave cladding-pumping technology introduced in this thesis brings down the cost of the amplifier by reducing the amount of components in the amplifier (pump WDM and gain flattening filter) and by requiring only a single low-cost multimode pump source. Furthermore the suppression of unwanted transient effects under the channel add/drop operation and the performance of the amplifier are enhanced by using a gain-clamping technique.

The application of inverse scattering design/modeling technique in conjunction with advanced fiber Bragg grating writing technique significantly reduces in-band dispersion and greatly improves grating characteristics. Using such techniques the filter amplitude response can be defined independently from its dispersion response. This was verified experimentally measuring the in-band dispersion penalty of a cascade of linear-phase fiber Bragg grating (FBG) filters and comparing the results with conventional apodized FBG filters. The network performance of such filters was further characterized by measuring the additional penalty on a dropped channel caused by a cascade of five adjacent channel gratings. Results imply that use of linear-phase FBG filters and FBG cascades result in a much wider usable bandwidth, which allows for an appreciably larger relative drift between the laser and filter central wavelengths. This relaxes the stability requirements and means that cheaper transmitter and packaging technologies can be used with beneficial overall system cost implications.

DFB fiber lasers are attractive alternatives to semiconductor lasers due to their fabrication simplicity, low relative intensity noise and high wavelength accuracy. The output power and efficiency of the DFB fiber lasers can be increased in master-oscillator-power-amplifier configurations. At the same time, however, other important characteristics affecting system performance such as OSNR and RIN are degraded. These performance trade-offs were studied adjusting the oscillator power and having different power amplifiers. It was found out that by adjusting the oscillator power and by designing the power amplifier correctly the efficiency of the DFB fiber laser can

be doubled while still retaining the RIN and the OSNR at the level of the commercially available semiconductor diodes.

Advanced in-fiber components can be used to build scalable metropolitan networks. The scalability of two such network architectures was analyzed by building experimental network set-ups and using a simulation tool. Results show that the scalability limitation imposed by the amplified RIN arising from the Rayleigh backscattering in bidirectional WDM ring networks can be avoided by using low gain shared-pump EDFAs and directly modulated transmitters. In high-density metropolitan WDM networks based on non-zero dispersion shifted fibers the main limiting nonlinearity is four-wave mixing. In metropolitan areas distributed Raman amplification (DRA) is the most effective means to reduce the effect of four-wave mixing.

8 References

[1] K. Fukuchi, T. Kasamatsu, M. Morie, R. Ohhira, T. Ito, K. Sekiya, D. Ogasawara, and T. Ono, "10.92-Tb/s (273 x 40-Gb/s) triple-band/ultra-dense WDM optical-repeated transmission experiment," in Proc. Optical Fiber Communications Conf. 2001 (OFC2001), Postdeadline Paper PD24, pp. PD24-1–PD-24-3.

[2] S. Bigo, Y. Frignac, G. Charlet, W. Idler, S. Borne, H. Gross, R. Dischler, W. Poehlmann, P. Tran, C. Simonneau, D. Bayart, G. Veith, A. Jourdan, and J. Hamaide, "10.2Tbit/s (256 x 42.7Gbit/s PDM/WDM) transmission over 100km TeraLight fiber with 1.28bit/s/Hz spectrum efficiency," in Proc. Optical Fiber Communications Conf. 2001 (OFC 2001), Post-deadline Paper PD25, pp. PD25-1–PD-25-3.

[3] C. Rasmussen, T. Fjelde, J. Bennike, F. Liu, S. Dey, B. Mikkelsen, P. Mamyshev, P. Serbe, P. van der Wagt, Y. Akasaka, D. Harris, D. Gapontsev, V. Ivshin, P. Reeves-Hall, "DWDM 40G transmission over trans-Pacific distance (10000 km) using CSRZ-DPSK, enhanced FEC and all-Raman amplified 100 km UltraWave fiber spans," in Proc. Optical Fiber Communications Conf. 2003 (OFC 2003), Post-deadline Paper PD18, pp. PD18-1–PD18-3.

[4] B. Zhu, L. E. Nelson, S. Stulz, A. H. Gnauck, C. Doerr, J. Leuthold, L. Grüner-Nielsen, M. O. Pedersen, J. Kim, R. Lingle, Y. Emori, Y. Ohki, N. Tsukiji, A. Oguri, and S. Namiki, "6.4-Tb/s (160x42.7 Gb/s) transmission with 0.8 bit/s/Hz spectral efficiency over 32x100 km of fiber using CSRZ-DPSK format," in Proc. Optical Fiber Communications Conf. 2003 (OFC 2003), Post-deadline Paper PD19, pp. PD19-1–PD19-3.

[5] H. M. Pask, R. J. Carman, D. C. Hanna, A. C. Tropper, C. J. Mackechnie, P. R. Barber, and J. M. Dawes, "Ytterbium-doped silica fiber lasers: Versatile sources for the 1-1.2 μm region, " IEEE J. of Selec. Topics in Q. Electr., vol. 1 no. 1, pp. 2-13, April 1995.

[6] J. Nilsson, J. K. Sahu, W. A. Clarkson, R. Selvas, A. B. Grudinin, S. Alam, "High-power fiber lasers: new developments," in Photonics West Conf. San Jose, CA, 2003, paper 4974-11.

[7] Limpert, A. Liem, T. Schreiber, H. Zellmer, A. Tünnermann, Friedrich Schiller, "Power and energy scaling of fiber laser systems based on ytterbium-doped large-mode-area fibers," in Photonics West Conf. San Jose, CA, 2003, paper 4974-22.

[8] J. D. Minelly, L. A. Zenteno, M. J. Dejneka, W. J. Miller, D. V. Kuksenkov, M. K. Davis, S. G. Crigler, and M. E. Bardo, "High power diode pumped single-transverse-mode Yb fiber laser operating at 978 nm", OFC'2000, Paper PD2, Baltimore, USA (2000).

[9] L. A. Zenteno, J. D. Minelly, A. Liu, J. G. Ellison, S. G. Crigler, D. T. Walton, D. V. Kuksenkov, and M. J. Deineka, "1 W single-transverse-mode Yb-doped double-clad fibre laser at 978 nm," Electron. Lett., Vol. 37, pp., 819, 2001.

[10] A. S. Kurkov, O. I. Medvedkov, V. M. Paramonov, S. A. Vasiliev, and E. M. Dianov, "High-power Yb-doped double-clad fiber lasers for range of 0.98-1.04 μm," in Proceedings of Optical Amplifiers and Their Applications, OWC2-1 (2001).

[11] K. H. Ylä-Jarkko, R. Selvas, D. B. S. Soh, J. K. Sahu, C. A. Codemard, J. Nilsson, S. A. Alam, and A. B. Grudinin, "A 3.5 W 977 nm cladding-pumped jacketed-air clad ytterbium-doped fiber laser," Advanced Solid-State Photonics conference 2003 (ASSP'03), San Antonio, Texas, 2-5 Feb. 2003, post-dead-line.

[12] R. Selvas, K. Ylä-Jarkko, S.-U. Alam, J. Nilsson, P. W. Turner, J. Moore, J. K. Sahu, A. B. Grudinin, "High Power 977 nm Fibre Sources Based on Jacketed Air-Clad Fibres," in Optical Fiber communication conference 2003 (OFC'2003), Atlanta, 23-28 March, 2003, paper TuL4, 2003.

[13] R. Paschotta, J. Nilsson, A. C. Tropper, and D. C. Hanna, "Ytterbium-doped fiber amplifiers," IEEE J. of Quantum Electr., vol. 33, no. 7, pp. 1049-1056, July 1997.

[14] J. Nilsson, J. D. Minelly, R. Paschotta, A. C. Tropper, and D. C. Hanna,"Ring-doped cladding-pumped single-mode three-level fiber laser," Opt. Lett. Vol. 23, no. 5, pp. 355-357, 1998.

[15] V. A. Kozlov, J. Hernandez-Cordero, R. L. Shubochkin, A. L. G. Carter, and T. F. Morse, "Silica-air double-clad optical fiber," IEEE Photonics Technol. Lett., vol. 12, no. 8, pp. 1007, 2000.

[16] A. B. Grudinin, J. Nilsson, P. W. Turner, C. C. Renaud, W. A. Clarkson, D. N. Payne, "Single clad coiled optical fibre for high power lasers and amplifiers," Proc. Conf. on Lasers and Electro-Optics, Baltimore, MD, US, 1999, post-deadline paper CPD26.

[17] D. J. DiGiovanni, and R. S. Windeler, "Article comprising an air-clad optical fiber," US patent 5907652, 1999.

[18] J. K. Sahu, C. C. Renaud, K. Furusawa, R. Selvas, J. A. Alvarez-Chavez, D. J. Richardson, and J. Nilsson, "Jacketed air-clad cladding-pumped ytterbium doped fibre laser with a wide tuning range," Electron. Lett., vol. 37, pp. 1116-1117, 2001.

[19] J. C. Knight, T. A. Birks, P. St. J. Russel, and D. M. Atkin, "All-silica single-mode optical fiber with photonic crystal cladding," Opt. Lett., vol. 21, no. 19, pp. 1547-1549, 1996.

[20] T. M. Monro, D. J. Richardson, and N. G. Broderick, "Efficient modeling of holey fibers," in Optical Fiber Communication Conf., San Diego, CA, Feb. 21-26, 1999, paper FG1.

[21] A. K. Srivastava, S. Radic, C. Wolf, J. C. Centanni, J. W. Sulhoff, K. Kantor, and Y. Sun, "Ultra-dense terabit capacity WDM transmission in L-band," in Optical Fiber Communication Conf., Anaheim, CA, 2000, PD27.

[22] H. Ono, M. Yamada, T. Kanamori, S. Sudo, Y. Ohishi, "1.58-μm band gain-flattened erbium-doped fiber amplifiers for WDM transmission systems," J. of Lightwave Technol. vol. 17, no. 3, pp. 490-496, Mar. 1999.

[23] J. Nilsson, S. Y. Yun, S. T. Hwang, J. M. Kim, and S. J. Kim, "Long wavelength erbium-doped fiber amplifier gain enhanced by ASE end-reflectors," IEEE Photon. Technol. Lett., vol. 10, no. 11, pp. 1551-1553, Nov. 1998.

[24] B. Min, H. Yoon, W. J. Lee, N. Park, "Coupled structure for wide-band EDFA with gain and noise figure improvements from C- to L-band ASE injection," IEEE Photon. Technol. Lett., vol. 12, no. 5, pp. 480-482, May 2000.

[25] J. F. Massicott, J. R. Armitage, R. Wyatt, B. J. Ainslie, and S. P. Craig-Ryan, "High gain, broadband, 1.6 μm Er^{3+} doped silica fiber amplifier," Electron. Lett., vol. 26, pp. 1645-1646, 1990.

[26] Y. Zhang, X. Liu, J. Peng, X. Feng, and W. Zhang, "Wavelength and power dependence of injected C-band laser on pump conversion efficiency of L-band EDFA," IEEE Photon. Technol. Lett., vol. 14, no. 3, pp. 290-293, Mar. 2002.

[27] B.-H. Choi, H.-H. Park, M. Chu, and S. K. Kim, "High-gain coefficient long-wavelength-band erbium-doped fiber amplifier using 1530-nm band pump," IEEE Photon. Technol. Lett., vol. 13, no. 2, pp. 109-111, Feb. 2001.

[28] F. A. Flood and C.C. Wang, "980-nm pump-band wavelength for long-wavelength-band erbium-doped fiber amplifiers," IEEE Photon. Technol. Lett., vol. 11, no. 10, pp. 1232-1234, Oct. 1999.

[29] P. Bousselet, M. Bettiati, L. Gasca, P. Lambelet, F. Leplingard, D. Bayart, "+30 dBm output power from cladding-pumped Yb-free EDFA for L-band applications", in Optical Amplifiers and its Applications (OAA'01), paper OWC3, 2001.

[30] M. Söderlund, S. Tammela, P Pöyhönen, M. Leppihalme, and N. Peyghambarian, "Amplified spontaneous emission in cladding-pumped L-band erbium doped fiber amplifiers," IEEE Photon. Technol. Lett., vol. 13, no. 11, pp. 22-24, Jan. 1999.

[31] C. Codemard, D. B. S. Soh, K. Ylä-Jarkko, J. K. Sahu, M. Laroche, and J. Nilsson, " Cladding-pumped L-band phosphosilicate erbium-ytterbium co-doped fiber amplifier," in Optical Amplifiers and its Applications (OAA'2003), Otaru, Japan, p. x.x, July, 2003.

[32] L. Zenteno, "High power double-clad fiber lasers," J. of Lightwave Technol. vol. 11, no. 9, pp. 1435-1446, Sep. 1993.

[33] C. Codemard, K. Ylä-Jarkko, J. Singleton, P. W. Turner, I. Godfrey, S.-U. Alam, J. Nilsson, J. Sahu, and A. B. Grudinin, "Low noise, intelligent cladding pumped L-band EDFA," in European Conference on Optical Communication (ECOC'02), PD1.7, Sept. 2002.

[34] N. N. Kharais, A. F. Elrefaie, R. E. Wagner, and S. Ahmed, "Performance of cascaded misaligned optical (de)multiplexers in multiwavelength optical networks," IEEE Photon. Technol. Lett., vol. 8, no. 8, pp. 1073-1075, Aug. 1996.

[35] G. Lenz, B. J. Eggleton, C. R. Giles, C. K. Madsen, and R. E. Slusher, "Dispersive properties of optical filters for WDM systems," IEEE, J. Quantum. Electron., vol. 34, pp. 1390-1402, Aug. 1998.

[36] B. J. Eggleton, G. Lenz, N. Litchinitser, D. B. Patterson, and R. E. Slusher, "Implications of fiber grating dispersion for WDM communication systems," IEEE Photon. Technol. Lett., vol. 9, no. 10, pp. 1403-1405, Oct. 1997.

[37] G. Lenz, B. J. Eggleton, C. K. Madsen, C. R. Giles, and G. Nykolak, "Optimal dispersion of optical filters for WDM systems," IEEE Photon. Technol. Lett., vol. 10, no. 4, pp. 567-569, Oct. 1997.

[38] G. Nykolak, B. J. Eggleton, G. Lenz, and T. A. Strasser, "Dispersion penalty measurements of narrow fiber Bragg gratings at 10 Gb/s," IEEE Photon. Technol. Lett., vol. 10, no. 9, pp. 1319-1321, Sept. 1998.

[39] M. Kuznetsov, N. M. Froberg, S. R. Henion, and K. A. Rauschenbach, "Power penalty for optical signals due to dispersion slope in WDM filter cascades," IEEE Photon. Technol. Lett., vol. 11 , no. 11, pp. 1411-1413, Nov. 1999.

[40] M. Kuznetsov, N. M. Froberg, S. R. Henion, C. Reinke, and C. Fennelly, "Dispersion-induced power penalty in fiber-Bragg-grating WDM filter cascades using optically preamplified and nonpreamplified receivers," IEEE Photon. Technol. Lett., vol. 12, no. 10, pp. 1406-1408, Oct. 2000.

[41] W. H. Loh, M. J. Cole, M. N. Zervas, S. Barcelos, and R. I. Laming, "Complex grating structures with uniform phase masks based on the moving fiber-scanning beam technique," Opt. Lett., vol. 20, no. 20, pp. 2051-2053, 1995.

[42] Y. Qiu, Y. Sheng, and C. Bealieu, "Optimal phase mask for fiber Bragg grating fabrication," J. of Lightwave Technol. vol. 17, no. 11, pp. 2366-2370, Nov. 1999.

[43] T. Komukai, K. Tamura, and M. Nakazawa, "An efficient 0.04-nm apodized fiber Bragg grating and its application to narrow-band spectral filtering," IEEE Photon. Technol. Lett., vol. 9, no. 7, pp. 934-936, July 1997.

[44] V. Mizrahi and J. E. Sipe, "Optical properties of photosensitive fiber phase gratings," J. of Lightwave Technol. vol. 11, no. 10, pp. 1513-1517, Oct. 1993.

[45] L. Wei and J. W. Y. Lit, "Phase-shifted Bragg grating filters with symmetrical structures," J. of Lightwave Technol. vol. 15, no. 8, pp. 1405-1410, Aug. 1997.

[46] A. Carballar, M. A. Muriel, and J. Azana, "Fiber grating filter for WDM systems: An improved design," IEEE Photon. Technol. Lett., vol. 11, no. 6, pp. 694-697, July 1999.

[47] K. O. Hill, and G. Meltz, "Fiber Bragg grating technology fundamental and overview," J. of Lightwave Technol. vol. 15, no. 8, pp. 1263-1276, Aug. 1997.

[48] T. Erdogan, "Fiber grating spectra," J. of Lightwave Technol. vol. 15, no. 8, pp. 1277-1294, Aug. 1997.

[49] C. R. Giles, "Lightwave applications of fiber Bragg gratings," J. of Lightwave Technol. vol. 15, no. 8, pp. 1391-1404, Aug. 1997.

[50] J. E. Sipe, I. Poladian, C. M. de Sterke, "Propagation through nonuniform grating structures," J. Opt. Soc. Amer. A, vol. 11, pp. 1307-1320, Apr. 1994.

[51] J. Skaar and K. M. Risvik, "A genetic algorithm for the inverse problem in synthesis of fiber gratings," J. of Lightwave Technol. vol. 16, no. 10, pp. 1928-1932, Oct. 1998.

[52] R. Feced, M. N. Zervas, and M. A. Muriel, "An efficient inverse scattering technique for the design of non-uniform fibre Bragg gratings," IEEE J. of Quantum Electron., vol. 35, pp. 1105-1115, Sept.-Oct. 1999.

[53] R. Feced and M. N. Zervas, "Effects of random phase and amplitude errors in optical fiber Bragg gratings," J. of Lightwave Technol. vol. 18, no. 1, pp. 90-101, Jan. 2000.

[54] J. Skaar, J. Wang and T. Erdogan, "On the synthesis of fiber Bragg gratings by layer peeling," IEEE J. of Quantum Electron., vol. 37, pp. 165-173, Feb. 2001.

[55] M. Ibsen, P. Petropoulos, M. N. Zervas, "Dispersion free fibre Bragg gratings," Proc. OFC'01, pp. MC1-1-3, 2001.

[56] S. Ryu, Y. Horiuchi, and K. Mochizuki, "Novel chromatic dispersion measurement method over continuous gigahertz tuning range," J. of Lightwave Technol., vol. 7, no. 8, pp. 1177-1180, Aug. 1989.

[57] J. T. Kringlebotn, P. R. Morkel, L. Reekie, J.-L. Archambault, and D. N. Payne, "Efficient diode-pumped single-frequency erbium:ytterbium fiber laser," IEEE Photon. Technol. Lett., vol. 5, no. 10, pp. 1162-1164, Oct. 1993.

[58] V. Mizrahi, D. J. DiGiovanni, R. M. Atkins, S. G. Grubb, Y.-K. Park, and J.-M. Delavaux, "Stable single-mode erbium fiber-grating laser for digital communication," J. of Lightwave Technol., vol. 11, no. 12, pp. 2021-2025, Dec. 1993.

[59] L. Dong, W. H. Loh, J. E. Caplen, and J. D. Minelly, "Efficient single-frequency fiber laser with novel photosensitive Er/Yb optical fibers," Opt. Lett., vol. 22, no. 10, pp. 694-696, May 1997.

[60] K. Hsu, W. H. Loh, L. Dong, and C. M. Miller, "Efficient and tunable Er/Yb fiber grating lasers," J. of Lightwave Technol., vol. 15, no. 8, pp. 1438-1441, Aug. 1997.

[61] J.-L. Archambault and S. G. Grubb, "Fiber gratings in lasers and amplifiers," J. of Lightwave Technol., vol. 15, no. 8, pp. 1378-1390, Aug. 1997.

[62] W. H. Loh, B. N. Samson, L. Dong, G. J. Cowle, and K. Hsu, "High performance single frequency fiber grating-based erbium:ytterbium-codoped fiber lasers," J. of Lightwave Technol., vol. 16, no. 1, pp. 114-118, Jan. 1998.

[63] H. N. Poulsen, P. Varming, A. Buxens, A. T. Clausen, I. Muñoz, P. Jeppesen, C. V. Poulsen, J. E. Pedersen, and L. Eskildsen, "1607 nm DFB fiber laser for optical communication in the L-band," in Proc. ECOC'99, Nice, France, September 1999, vol. 1, pp. 70-71.

[64] M. Ding, and P. K. Cheo, "Analysis Er-doped fiber laser stability by suppressing relaxation oscillations," IEEE Photon. Technol. Lett., vol. 8, no. 9, pp. 1151-1153, Sept. 1996.

[65] T. Tellert, F. Di Pasquale, and M. Federighi, "Theoretical analysis of the dynamic behavior of highly-efficient Er/Yb codoped fiber lasers," IEEE Photon. Technol. Lett., vol. 8, no. 11, pp. 1462-1464, Nov. 1996.

[66] S. Taccheo, P. Laporta, O. Svelto, and G. De Geronimo, "Intensity noise reduction in a single-frequency ytterbium-codoped erbium laser," Opt. Lett., vol. 21, no. 21, pp. 1747-1749, Nov. 1996.

[67] H. L. An, E. Y. B. Pun, X. Z. Lin, and H. D. Liu, "Effects of ion clusters on the intensity noise of heavily erbium-doped fiber lasers," IEEE Photon. Technol. Lett., vol. 11, no. 7, pp. 803-805, July. 1999.

[68] H. L. An, X. Z. Lin, and H. D. Liu, "Intensity-noise suppression by ytterbium codoping in heavily erbium-doped fiber lasers with partly clustered erbium ions," Opt. Lett., vol. 25, no. 24, pp. 1747-1749, 2000.

[69] H. Shi, D. Cohen, J. Barton, M. Majewski, L. A. Coldren, M. C. Larson, and G. A. Fish, "Relative intensity noise measurements of a widely tunable sampled-grating DBR laser," IEEE Photon. Technol. Lett., vol. 14, no. 6, pp. 759-761, June 2002.

[70] G. A. Ball, C. E. Holton, G. Hull-Allen, and W. W. Morey, "60 mW 1.5 mm single-frequency low-noise fiber laser MOPA," IEEE Photon. Technol. Lett., vol. 6, no. 2, pp. 192-194, Feb. 1994.

[71] J. J. Pan, and Y. Shi, “166-mW single-frequency output power interactive fiber lasers with low noise,” IEEE Photon. Technol. Lett., vol. 11, no. 1, pp. 36-38, Jan. 1999.

[72] Winston I. Way, Broadband Hybrid Fiber/Coax Access System Technologies, Academic Press, San Diego, pp. 315, 1999.

[73] J. B. Stark, M. C. Nuss, W. H. Knox, S. T. Cundiff, L. Boivin, S. G. Grubb, D. Tipton, D. DiGiovanni, U. Koren, and K. Dreyer, “Cascaded WDM passive optical network with a highly shared source,” IEEE Photon. Technol. Lett., vol. 9, no. 8, pp. 1170-1172, Aug. 1997.

[74] N. J. Frigo, P. P. Iannone, P. D. Magill, T. E. Darcie, M. M. Downs, B. N. Desai, U. Koren, T. L. Koch, C. Dragone, H. M. Presby, and G. E. Bodep, “A wavelength-division multiplexed passive optical network with cost-shared components,” IEEE Photon. Technol. Lett., vol. 6, no. 11, pp. 1365-1367, Nov. 1994.

[75] X. P. Mao, R. W. Tkach, A. R. Charplyvy, R. M. Jopson, and R. M. Derosier, “Stimulated Brillouin threshold dependence on fiber type and uniformity,” IEEE Photon. Technol. Lett., vol. 4, no. 1, pp. 66-69, 1992.

[76] S. A. Alam, K. H. Ylä-Jarkko, and A. B. Grudinin, “High power, single frequency DFB fibre laser with low relative intensity noise,” in European Conference on Lasers and Electro-Optics and the European Quantum Electronics Conference (CLEO®/Europe—EQEC 2003), Munchen, 23-27 June 2003.

[77] A.A. Saleh and J. M. Simmons, “Architectural principles of optical regional and metropolitan access networks,” Journal of Lightwave Technology, vol. 17, no. 12, (Dec. 1999), pp. 2431-2448.

[78] I. Tomkos, R. Hesse, C. Friedman, N. Antonides, N. Madamopoulos, B. Hallock, R. Vodhanel, and A. Boskovic, “Transport performance of a transparent WDM regional area ring network utilizing optimised components/fiber,” Optical Fiber Communication Conference (OFC), Anaheim, U.S., 17-22 March 2001, pp. PD35-1 -PD35-3, vol.4.

[79] N. Madamopoulos, D. C. Friedman, I. Tomkos, and A. Boskovic, “Study of the performance of a transparent and reconfigurable metropolitan area network,” J. of Lightwave Technol. vol. 20, no. 6, pp. 937-945, June 2002.

[80] E. Lowe, “Current European WDM deployment trends,” IEEE Communications Magazine, vol. 36, no. 2, (Feb. 1998), pp. 46-50.

[81] J. Bannister, M. Gerla, and M. Kovačević, “An all optical multifiber tree network,” INFOCOM'93, (San Francisco, CA, USA, April 1993), vol. 1, pp. 282-292.

[82] N. Nagatsu, A. Watanabe, S. Okamoto, and K. Sato, “Architectural analysis of multiple fiber ring networks employing optical paths,” J. of Lightwave Technol, vol. 15, no. 10, (Oct. 1997), pp. 1794-1804.

[83] H. Obara, H. Masuda, K. Suzuki, and K. Aida, “Multifiber wavelength division multiplexed ring network architecture for tera-bit/s throughput,” Proc. IEEE of ICC'98, (Atlanta, GA, June 1998), vol. 2, pp. 921-925.

[84] K.-P. Ho, S.-K. Liaw, and C. Lin, “Performance of an eight-wavelength bidirectional WDM add/drop multiplexer with 80-Gbit/s capacity,” Proc. of OFC'97, (Dallas, Texas, USA, Feb. 1997), pp. 90-91.

[85] H. Obara, H. Masuda, and K. Aida, “Transmission over a 200-km single-fiber bidirectional ring network with reconfigurable add/drop repeaters,” Proc. of ECOC'97, (Edinburgh, Scotland, Sep., 1997), pp. 9-12.

[86] C.H. Kim, C.-H. Lee, and Y.C. Chung, “Bidirectional WDM self-healing ring network based on simple bidirectional add/drop amplifier modules,” IEEE Photonics Technology Letters, vol. 10, no. 9, (Sep. 1998), pp. 1340-1342.

[87] Y. Zhao, X. J. Zhao, J. H. Chen, F. S. Choa, and Y. J. Chen, “A novel bidirectional add/drop module for single fiber bi-directional self-healing wavelength division multiplexed ring networks,” Proc. of OFC'99, (San Diego, CA, Feb. 1999), pp. 183-185, Feb. 1999.

[88] S. Tammela, J. Aarnio, and A. Tervonen, “Survivable WDM/SDM ring for metropolitan networks,” Proc. of SPIE, vol. 3531, (1998), pp. 448-454.

[89] K. Ylä-Jarkko, S. Tammela, and A. Tervonen, “Bidirectional WDM multifiber ring network with shared-pump EDFAs,” Proc. ECOC'99, (Nice, France, Sep. 1999), vol.1, pp. 46-47.

[90] K. Ylä-Jarkko, S. Tammela, T. Niemi, and A. Tervonen, “Scalability of a multifiber bidirectional metropolitan WDM ring network,” Proc. of ECOC'00, (München, Germany, Sep. 2000), vol. 3, pp. 81-82.

[91] L. Gimlett and N. K. Cheung, “Effects of phase-to-intensity noise conversion by multiple reflections on gigabit-per-second DFB laser transmission systems,” J. of Lightwave Technol., vol. 7, no. 6, pp. 888-895, June 1989.

[92] L. Gimlett, M. Z. Iqbal, L. Curtis, and N. K. Cheung, “Impact of multiple reflection noise in Gbit/s lightwave systems with optical amplifiers,” IEE Electronic Letters, vol. 25, no. 20, pp. 1393-1394, Sept. 1989.

[93] J. L. Gimlett, M. Z. Iqbal, N. K. Cheung, A. Righetti, F. Fontana, and G. Grasso, “Observation of equivalent Rayleigh scattering mirrors in lightwave systems with optical amplifiers,” IEEE Photonics Technol. Lett., vol. 2, no. 3, pp. 211-213, Mar. 1990.

[94] P. Wan and J. Conradi, “Impact of double Rayleigh backscatter noise on digital and analog fiber systems,” J. of Lightwave Technol., vol. 14, no. 3, pp. 288-297, Mar. 1996.

[95] M. O. van Deventer, “Polarization properties of Rayleigh backscattering in single-mode fibers,” J. of Lightwave Technol., vol. 11, no. 12, pp. 1895-1899, Dec. 1993.

[96] R. K. Staubli and P. Gysel, “Crosstalk penalties due to coherent Rayleigh noise in bidirectional optical communication systems,” J. of Lightwave Technol., vol. 9, no. 3, pp. 375-380, Mar. 1991.

[97] P. J. Legg, M. Tur, and I. Andonovic, “Solution paths to limit interferometric noise induced performance degradation in ASK/direct detection lightwave networks,” J. of Lightwave Technol., vol. 14, no. 9, pp. 1943-1953, Sept. 1996.

[98] T. Niemi, S. Tammela, T. Kajava, M. Kaivola, and H. Ludvigsen, “Temperature-tunable silicon-wafer etalon for frequency chirp measurements,” Microwave and Optical Technol. Lett., vol. 20, no. 2, pp. 190-192, Feb. 1999.

[99] A. R. Chraplyvy, “Limitations on lightwave communications imposed by optical-fiber nonlinearities”, J. Lightwave Technol., vol. 8, no. 10, pp. 1548-1557, Oct. 1990.

[100] M. Eiselt, L. D. Garrett, and R. W. Tkach, “Experimental comparison of WDM system capacity in conventional and nonzero dispersion shifted fiber,” IEEE Photon. Technol. Lett., vol. 11, no. 2, pp. 281-283, Feb. 1999

[101] Y. Aoki, K. Tajima, and I. Mito, ”Input power limits of single-mode optical fibers due to stimulated Brillouin scattering in optical communication systems,” J. Lightwave Technol., vol. 6, no. 5, pp. 710-719, May 1988.

[102] X. P. Mao, R. W. Tkach, A. R. Chraplyvy, R. M. Jopson, and R. M. Derosier, “Stimulated Brillouin threshold dependence on fiber type and uniformity,” IEEE Photon. Technol. Lett., vol. 4, no. 1, pp. 66-69, Jan. 1992.

[103] D. A. Fishman, and J. A. Nagel, “Degradations due to stimulated Brillouin scattering in multigigabit intensity-modulated fiber-optic systems,” J. Lightwave Technol., vol. 11, no. 11, pp. 1721-1728, Nov. 1993.

[104] K. Shiraki, M. Ohashi, and M. Tateda, “SBS threshold of a fiber with a Brillouin frequency shift distribution,” J. Lightwave Technol., vol. 14, no. 1, pp. 50-57, Jan. 1996.

[105] M. M. Howerton, W.K. Burns, and G. K. Gopalakrishnan, “SBS suppression using a depolarized source for high power fiber applications,” J. Lightwave Technol., vol. 14, no. 3, pp. 417-422, Mar. 1996.

[106] M. Niklès, L. Thévenaz, and P. A. Robert, “Brillouin gain spectrum characterization in single-mode optical fibers,” J. Lightwave Technol., vol. 15, no. 10, pp. 1842-1851, Oct. 1997.

[107] C. C. Lee, “Measurement of stimulated-Brillouin-scattering threshold for various types of fibers using Brillouin-optical-time-domain reflectrometer,” IEEE Photon. Technol. Lett., vol. 12, no. 6, pp. 672-674, June 2000.

[108] F. Forghieri, R. W. Tkach, and R. Chraplyvy, “WDM systems with unequally spaced channels,” J. Lightwave Technol., vol. 13, no. 5, pp. 889-897, 1995.

[109] K. Inoue, “Arrangement of orthogonal polarized signals for suppressing fiber four-wave mixing in optical multichannel transmission systems,” IEEE Photon. Technol. Lett., vol. 3, no. 6, pp. 560-563, 1991.

[110] M. Eiselt, “Limits on WDM systems due to four-wave mixing: a statistical approach,” J. Lightwave Technol., vol. 17, no. 11, pp. 2261-2267, 1999.